Chapter 3: Deformation Behavior and Tribo-Mechanical Properties of the Complex Hypereutectic Al-18Si-2.5Cu-0.6Fe alloy during Forging

3.1 Introduction

Various automotive and aerospace components are subjected to severe working conditions consequently reduces the power transmission, working efficiency and causes catastrophic failure of the components. Such stringent requirements of automotive and aerospace industries have prompted the development of newer materials with high strength to weight ratio, low coefficient of thermal expansion and high wear and corrosion resistance. Therefore, numerous efforts have been made to produce materials with excellent wear resistance characteristics. These efforts include alloying of elements, different production techniques, and surface treatment. Hypereutectic aluminum-silicon alloys are such material which possesses the high strength to weight ratio, low density, and excellent wear resistance. So, it is successfully being used in producing different automotive components and aerospace engine parts (Wang et al., 2016, Lu and Zhang, 2017, Yu et al., 2018).

The higher amount of silicon content in conventionally cast hypereutectic Al-Si alloys often produces coarse primary Si along with needle-shaped eutectic Si particles. Therefore, numerous investigations have been performed to alteration of these microstructures by using different modifiers and/or refiners or various heat treatment techniques (Zuo et al., 2010; Shivaprasad et al., 2015). But the components produced through this technique have insufficient strength and require long heat treatment cycles. Processing of Al-Si alloy through bulk metal forming techniques such as forging (Murali and Yong, 2010, Cai et al., 2015), extrusion (Ke et al., 2010, Liang et al., 2016) and

rolling (Umezawa and Nagai, 1999) is a convenient way to produce sound products with excellent mechanical properties. Bulk processing improves the tribo-mechanical performance of the alloy by altering the coarse microstructural features to refined particles. However, bulk processing of alloy is very difficult due to the presence of hard silicon particles as it reduces the ductility of the alloy and often produces surface cracks on the products (Kang et al., 1999). Therefore, process parameters such as compression load, processing velocity, processing temperature, deformation ratio, solidification rate, size of the alloying elements affect the bulk processing of the material which in turn affects its tribo-mechanical properties. Therefore, careful selection of these parameters is needed to obtain promising results.

In view of the above facts, the generation of cracks in Al-Si alloys is a major concern during bulk processing and thus attracted the attention of researchers towards this issue to produce defect-free products. The present investigations have been undertaken to explore the feasibility of bulk processing of complex Al-18Si-2.5Cu-0.6Fe and also study the effect of various processing parameters on tribo-mechanical behavior. The alloy forged through open die set, impression die set and converging die under different deforming conditions, working temperatures, and frictional conditions. The present work provides valuable insight into the deformation behavior and tribo-mechanical characteristics of the Al-18Si-2.5Cu-0.6Fe (wt.%) alloy under different processing conditions.

3.2 Results and Discussion

3.2.1 Microstructural features of the as-cast alloy

The x-ray diffraction (XRD) patterns of the as-cast Al-18Si-2.5Cu-0.6Fe alloy is shown in Figure 3.1. The phases present in the alloys have been identified using the International Centre for Diffraction Data (ICDD) PDF database. The high-intensity peaks

corresponding to aluminum and silicon phases are quite distinct in the XRD patterns. Diffraction peaks related to intermetallics β-$Al_{4.5}FeSi$ and Al_2Cu are also evident from the XRD patterns. However, the intensity of the peaks corresponding to intermetallics is weak. The formation of the intermetallic compounds may be ascribed to exposure of the material at high temperature during melting which promoted interfacial reactions between the matrix and the alloying elements. Therefore, due to the presence of silicon, copper, and iron in the alloys, the intermetallic compounds may be formed either rich in silicon or copper or iron coexisting in the Al matrix.

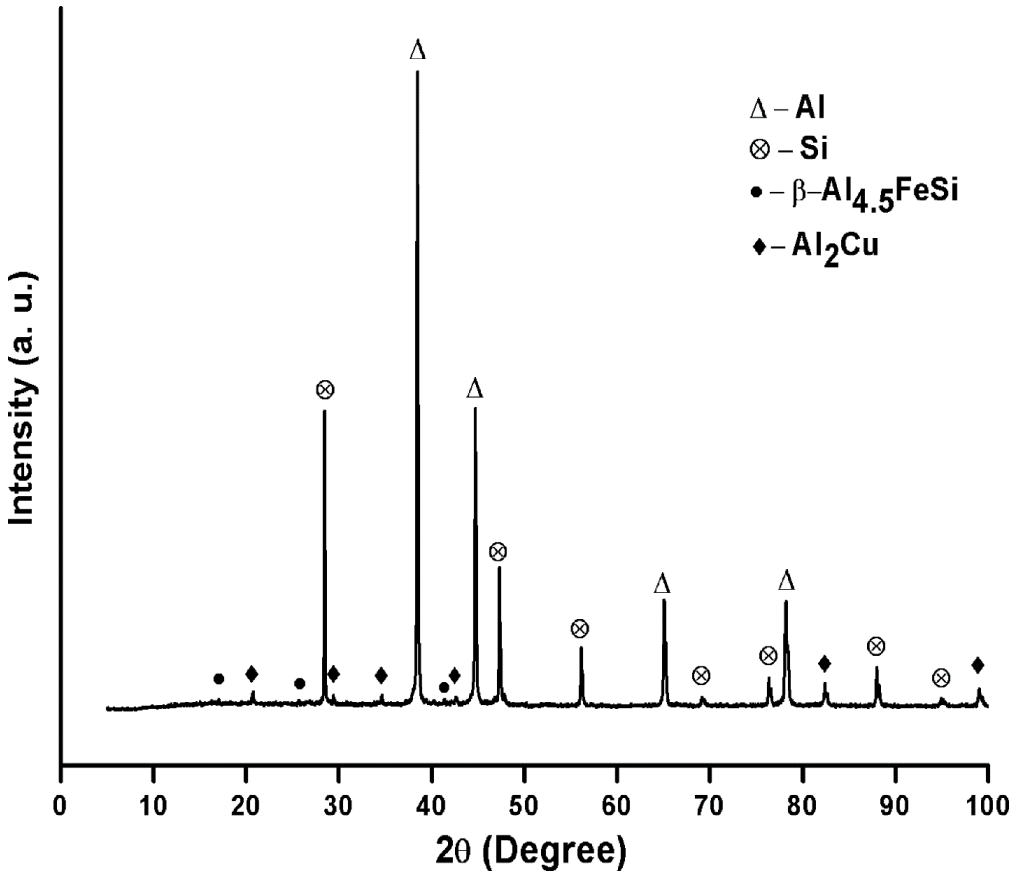

Figure 3.1 X-ray diffraction (XRD) patterns of the as-cast alloy

The EDAX spectrum of the as-cast alloy was taken from the area observed in the SEM images as shown in Figure 3.2(a). EDAX analysis indicates the presence of the Al, Si, Cu, Fe, Mg and Zn elements; refer Figure 3.2(b) in the alloy. EDAX spectrum further confirmed the formation of intermetallic phases (Al_2Cu and β-$Al_{4.5}FeSi$); refer Figures

3.2(c) and 3.2(d). SEM micrograph shows the presence of plate type and coarse needle-shaped intermetallic phases. Figure 3.2(e) shows the EDAX spectrum of Si crystal.

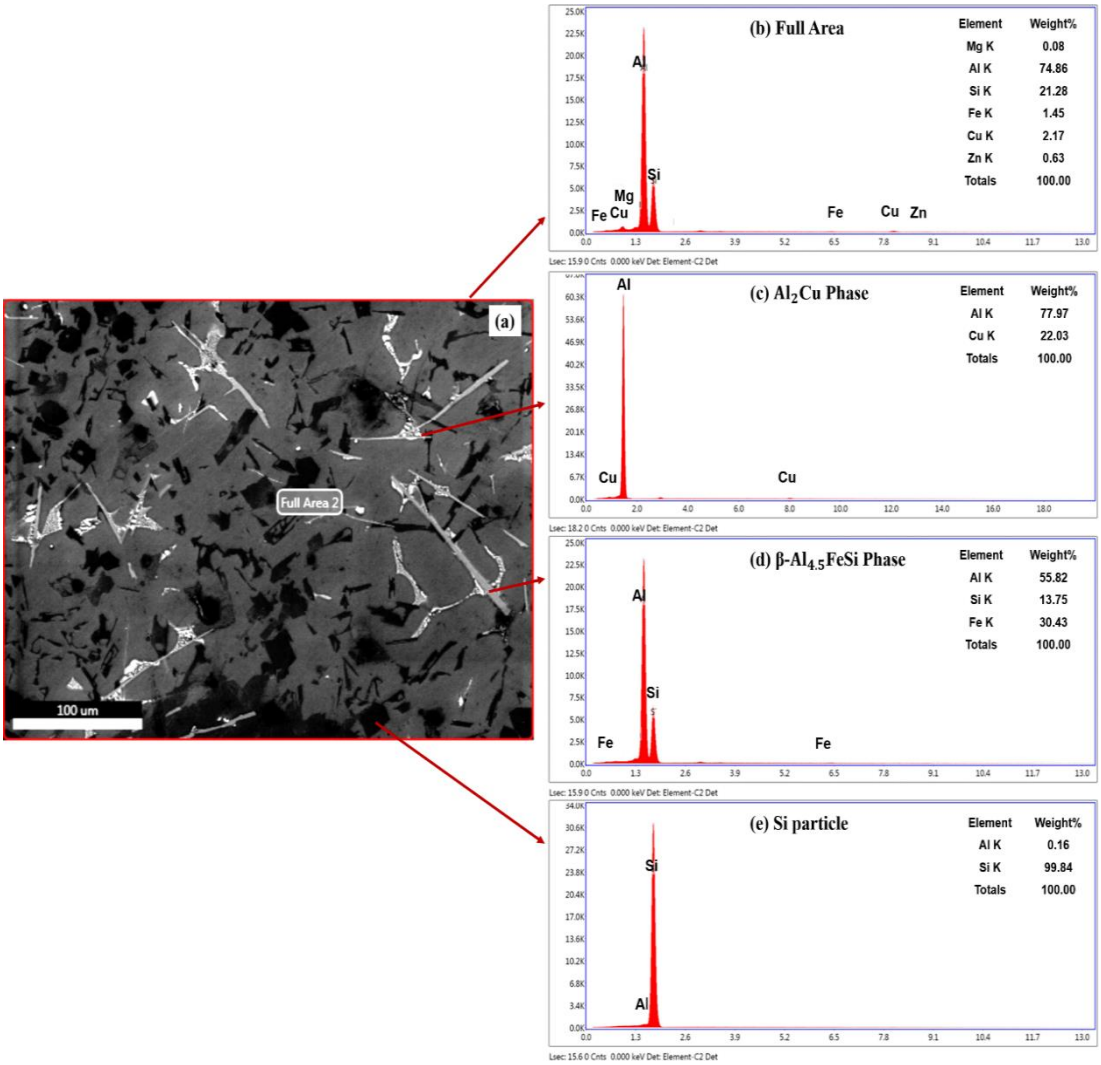

Figure 3.2 EDAX analysis of the as-cast alloy

Figure 3.3 shows the optical micrograph of the as-cast alloy. The microstructure of the as-cast alloy exhibits coarse irregular primary silicon particles along with needle-shaped silicon particles. These constituents of eutectic phases are randomly oriented and non-uniformly distributed in the aluminum matrix. The formation and distribution of such silicon phases occur due to non-uniformity in cooling rate during the solidification process. The mean diameter/standard deviation of the primary silicon particles is measured as 41.90/25.80 µm while 39.60/15.20 µm for eutectic silicon.

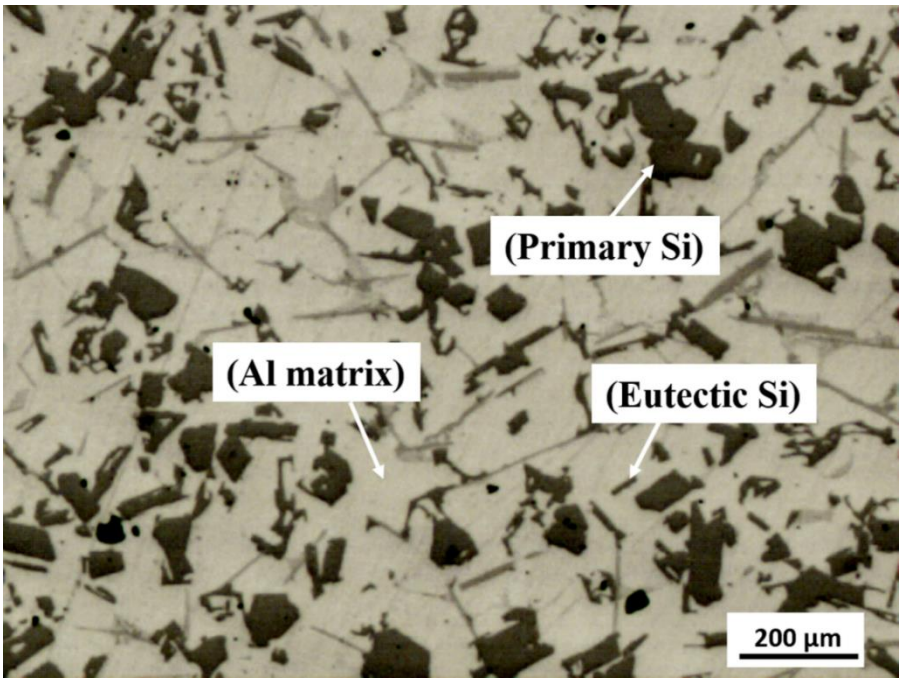

Figure 3.3 Optical microstructure of the as-cast alloy

3.2.2 Deformation behavior of the complex hypereutectic Al-18Si-2.5Cu-0.6Fe alloy forged under different die sets

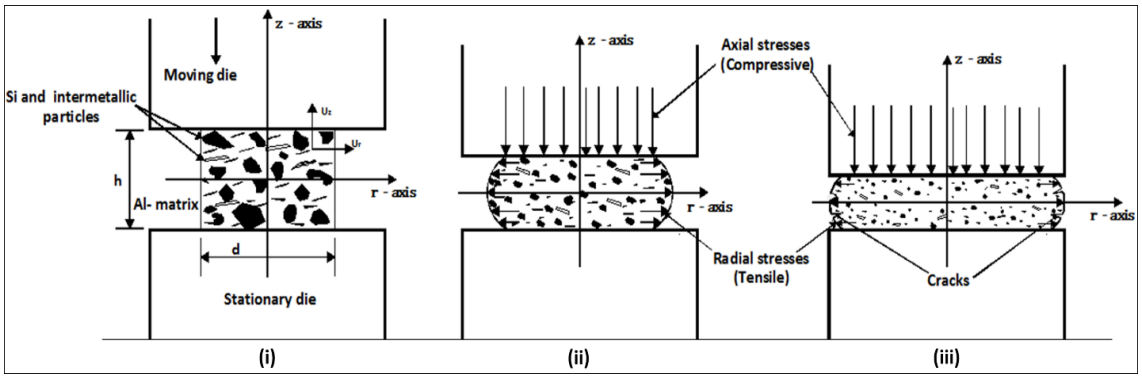

Figure 3.4 Three regimes of silicon-intermetallic particles distribution with aluminum matrix during open die forging of the complex Al-Si alloy

The feasibility of the bulk processing of the complex Al-18Si-2.5Cu-0.6Fe alloy has been investigated and the deformation behavior of the alloy has been critically analyzed. The bulk processing was performed through the forging process under different die setups namely open die, impression die, and converging die sets. The test samples were forged under various processing conditions of working temperatures and lubrication. Figure 3.4

shows the three regimes of silicon-intermetallic particles distribution in the aluminum matrix during open die forging of Al-Si alloy.

3.2.2.1 Deformation behavior of the complex hypereutectic Al-Si alloy during open die forging

The open die forging of the test samples (h/d=1) was performed on power at room temperature and 300°C. The results reveal that open die forging of the complex hypereutectic Al-Si alloy test samples (h/d=1) developed severe surface cracks on the outer periphery in both room and elevated working temperatures (300°C) and the same can be seen in Figures 3.5(a-b).

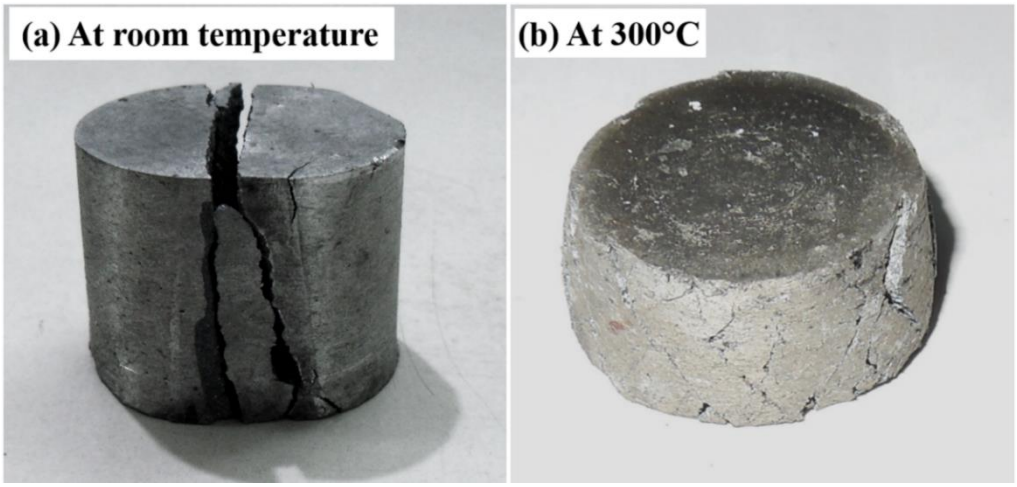

Figure 3.5 Open die forged products under different working condition (a) room temperature, (b) 300°C

During open die forging of the alloy at room temperature, the hard silicon, and intermetallic particles; which are brittle, fail to sustain high axial (compressive), and radial (tensile) stresses during deformation. Due to ineffective recovery and increased flow stresses, the stress concentration initiates between regions of silicon-intermetallic particles and aluminum matrix. As a result, macro separation gradually appears in the interface region, and this further leads to severe cracks on the equatorial free surface as shown in Figure 3.5(a). However, open die forging of the alloy carried out at 300°C temperature and high strain rate, the recovery process occurs substantially and thus

enabling large strains with no strain hardening effect. Due to high axial (compressive) and radial (tensile) stresses, the hard silicon and intermetallic particles tend to fracture and fragmented along with plastically deformed soft Al matrix during forging. The fragmented particles tend to flow laterally along with soft aluminum matrix; extruding into the voids created by the cracking and also generates stress concentration along with the Al matrix. Further, the recovery process of the soft outward flowing metal is incomplete due to macro-separation appearing between the solid and liquid regions as seen in Figure 3.5(b). Previously, Kang et al., 1999 also reported that the outer surface of sample cracked and fractured during compression forming of the A356 alloy.

In view of the above discussion, it is established that the open die forging of the complex Al-18Si-2.5Cu-0.6Fe alloy is not feasible both in room and elevated temperatures. The above results motivated to investigate high speed impression die forging of the Al-18Si-2.5Cu-0.6Fe alloy at room and elevated working temperatures.

3.2.2.2 Deformation behavior of the complex hypereutectic Al-Si alloy during impression die forging at room temperature

During the impression die forging, the large axial compressive stresses act vertically on the preform. Consequently, the compression process proceeds causing the preform to barrell due to interfacial friction, and thus the plastically deformed material starts flowing radially outward. During the initial part of the loading, the preform undergoes severe axial bulk deformation along with height and relatively less radial metal flow which gradually starts filling the die. This radial (tensile) stresses initiate cracks between needles shaped second phase particles and Al matrix, which further propagate during processing. As a result of this, the preform got fractured and fragmented during processing with insignificant metal deformation.

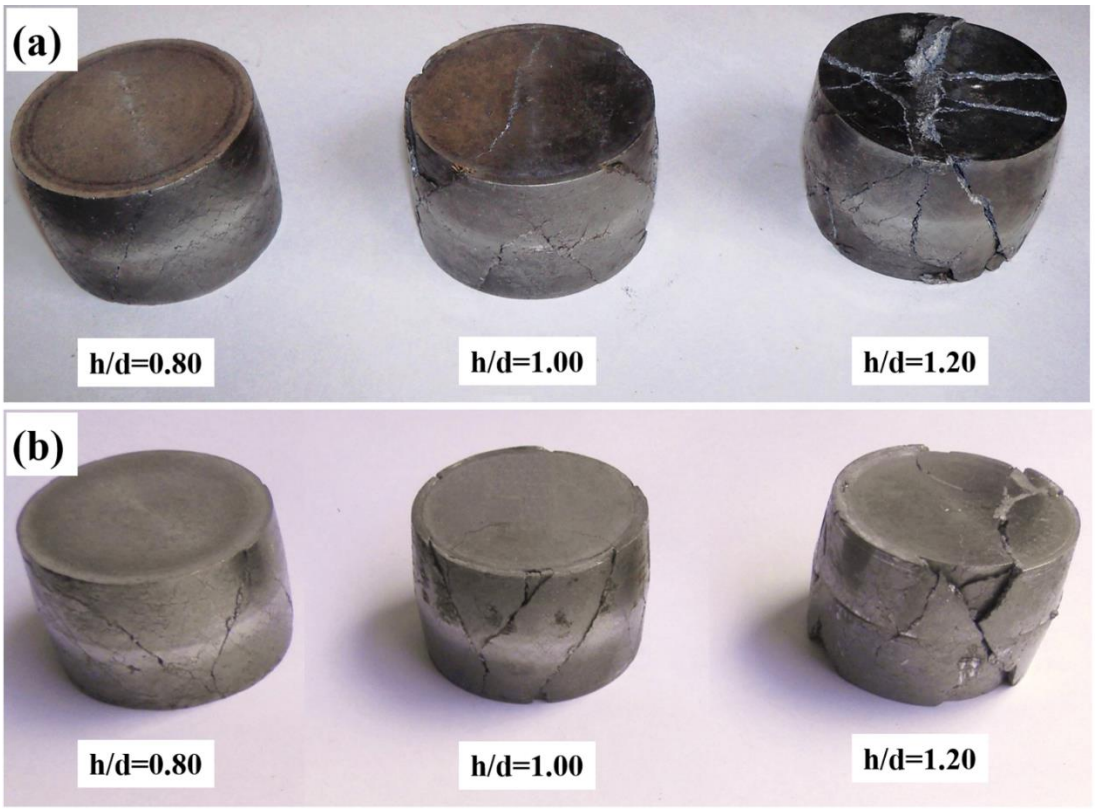

Figure 3.6 Photograph forged preform under interfacial frictional conditions with different aspect ratios (a) lubricated, and (b) unlubricated

Figures 3.6(a-b) shows the photograph of Al-Si alloy preforms forged under lubricated and unlubricated interfacial frictional conditions with aspect ratios of 0.80, 1.00 and 1.20. The preform with an aspect ratio 0.80 shows minute cracks on the equatorial surface after compression, whereas preform with high aspect ratios (1.20 and 1.00) show severe surface cracks. Thus, the preforms with large aspect ratios (1.20 and 1.00) develop cracks on the barrelled surface which flows radially outward towards the die wall. Unfortunately, due to severe cracking, the back (compressive) stresses are incapable to develop highly oriented strong crack free surface. On the other hand, the Al-Si preform with aspect ratio 0.80 undergoes controlled amount of axial (compressive) stresses, radial (tensile) stresses and also back (compressive) stresses from die walls and consequently produce a forged product with few minute surface cracks.

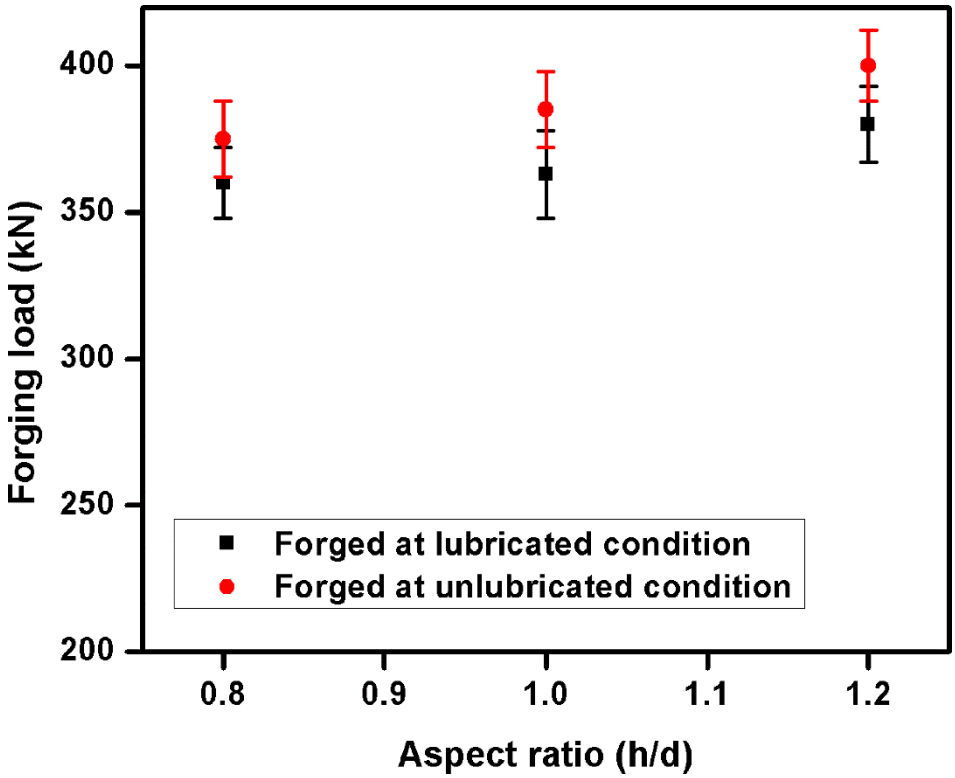

Figure 3.7 Variation of forging load with aspect ratio (h/d) at lubricated and lubricated conditions

Figure 3.7 shows the variation of load with aspect ratio during the forging of the alloy under lubricated and unlubricated interfacial frictional conditions. The results reveal that samples forged at lubricated condition required less deformation load as compared with unlubricated conditions. It may due to less surface movement between die wall and preform led to barreling of the preform during forging, requires higher forging load to proceed the deformation and fill the die cavity. The results also show that the deformation load increases with an increase in aspect ratio, and higher for the test samples with h/d=1.20 in both frictional conditions. It may be due to the fact that percentage height reduction was higher for the samples with h/d=1.20 (35%) than other which demand greater load to deform the test samples

It is evident from the above discussion that the aspect ratio (h/d) plays a significant role in the preform designing, and in turn dictates the metal flow pattern through an impression die set. During impression die forging the Al-Si alloy preform with aspect

ratios 1.20 and 1.00 undergoes both unrestricted and restricted metal flow during compression, whereas restricted metal flow dominates the die filling due to a relatively less radial clearance between die wall and the preform (h/d=0.80). Obviously, this metal flow phenomenon of the preform with aspect ratio 0.80 greatly affects the mechanical and metallurgical properties of the forged products.

In view of the above discussion, it is established that the impression die forging of the complex Al-18Si-2.5Cu-0.6Fe alloy is not feasible at room temperature, and the products got cracked and fractures during processing. The above results motivated the authors to investigate the forging of the Al-18Si-2.5Cu-0.6Fe alloy through impression die at elevated processing temperatures.

3.2.2.3 Deformation behavior of the complex hypereutectic Al-Si alloy during impression die forging at elevated working temperatures

The impression die forging of the test samples were performed through power hammer at elevated temperatures (300, 400, and 500°C) under lubricated and unlubricated interfacial friction conditions.

During compression of the alloy at elevated temperatures (300, 400, and 500°C), the soft Al matrix deforms plastically while the hard second phase particles fractured and fragmented, and gets dispersed in the matrix. Forging of the Al-Si alloy at elevated temperatures induced ductility and thus soften the material. During impression die forging, the large axial stresses which are compressive in nature act vertically on the preform. As a result, the deformation begins and material starts flowing in the outward direction due to radial stresses (tensile) on the plastically deformed material. Thus, initially the preform undergoes severe axial bulk deformation and relatively little radial deformation. Gradually the outward flowing metal encounters the die walls which produce back stresses against radially outward flowing material. Consequently, the weak

structure of brittle polyhedral and needle shaped Si particles and intermetallic phase gets fractured and fragmented, resulting re-oriented strong structure during the forging process. Since second phase particles initiate surface cracks on the outer periphery of deformed samples during forging but the previously developed back stresses protect the surface against cracks. The above phenomenon of metal flow produces the product with a better surface finish. Therefore, impression die forging of the above alloy produce crack-free products with a smooth surface as shown in Figures 3.8 (a-b) and 3.9 (a-c).

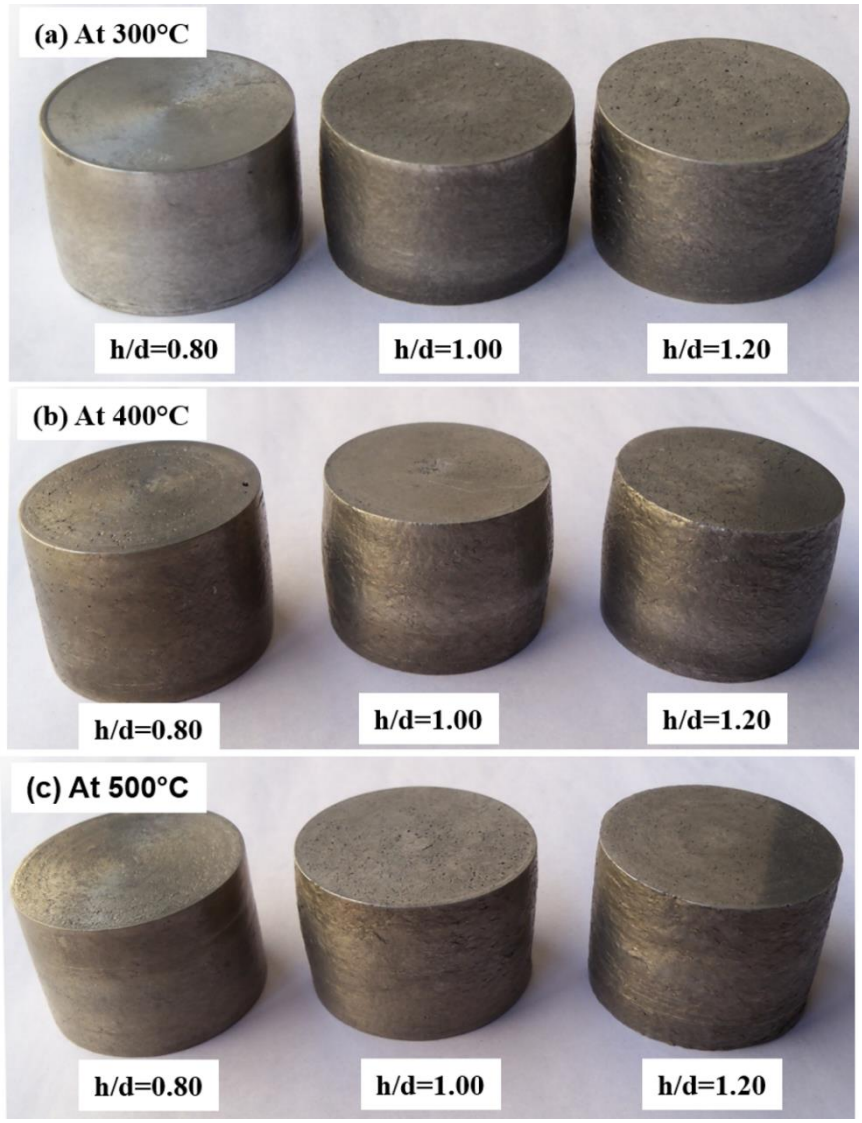

Figure 3.8 Photograph of impression die forged products under lubricated condition at elevated processing temperature (a) 300°C, (b) 400°C, and (c) 500°C

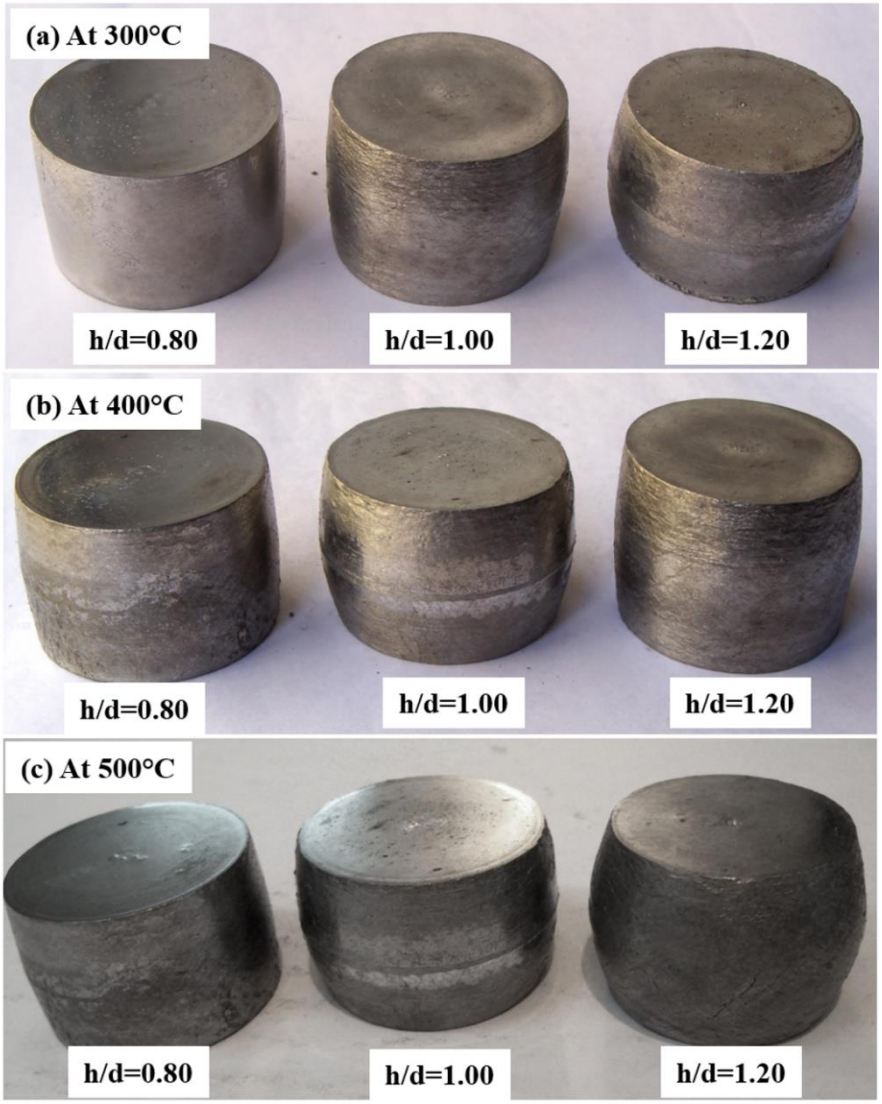

Figure 3.9 Photograph of impression die forged products under unlubricated condition at elevated processing temperature (a) 300°C, (b) 400°C, and (c) 500°C

The results show that lubricated forging condition produces a better surface finish then unlubricated condition. It may be due lubricant reduces the friction between die and preform surface during processing, and thus produces a product with smooth surface. In impression die forging, the design dimensions of the preform play an important role as it decides the metal flow pattern during bulk processing which affects the quality of the final forged product. The test sample with h/d=1.20 undergoes severe axial and radial bulk deformation both till the outward flowing metal encounters the die wall. For h/d=0.80, the preform undergoes severe bulk axial, and little radial deformation and

shortly the outward flowing metal encounters the die walls due to the large diameter of the preform. The Test sample with h/d=1.0 is an intermediate situation.

Figures 3.10 and 3.11 show variation of forging load with the aspect ratio (h/d) at different working temperatures during impression die forging of Al-18Si-2.5Cu-0.6Fe alloy under lubricated and unlubricated conditions. From Figures 3.10 and 3.11, it is evident that the forging load increases with the increase in aspect ratio at all working temperatures under both lubricated and unlubricated conditions. This is because of axial stresses play a dominant role during deformation of the test samples having h/d=0.80 whereas for h/d=1.20 and 1.0 both the axial and radial stresses are significant for complete die filling. Since the samples having h/d=1.0 needs relatively small axial compression and lateral spread for complete die filling, therefore less forging load is required as compared to h/d=1.20. Due to softening of the alloy at the higher temperature (500°C), the test samples required relatively low forging load to deform the material in all different cases of aspect ratios under lubricated and unlubricated conditions.

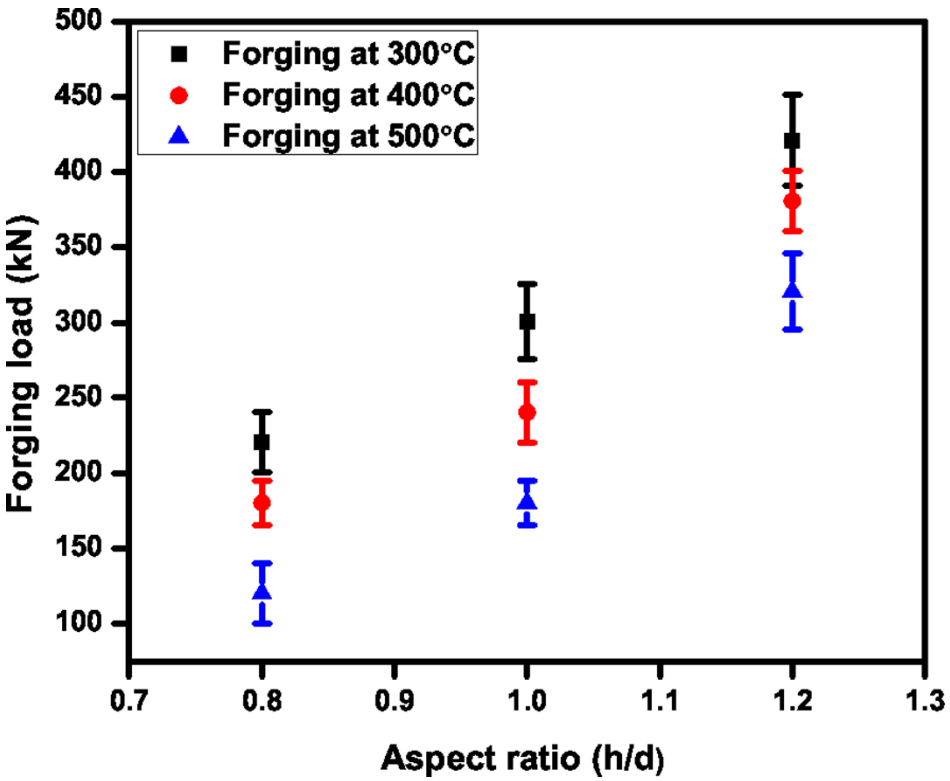

Figure 3.10 Variation of forging load with aspect ratio (h/d) at different working temperatures under lubricated condition

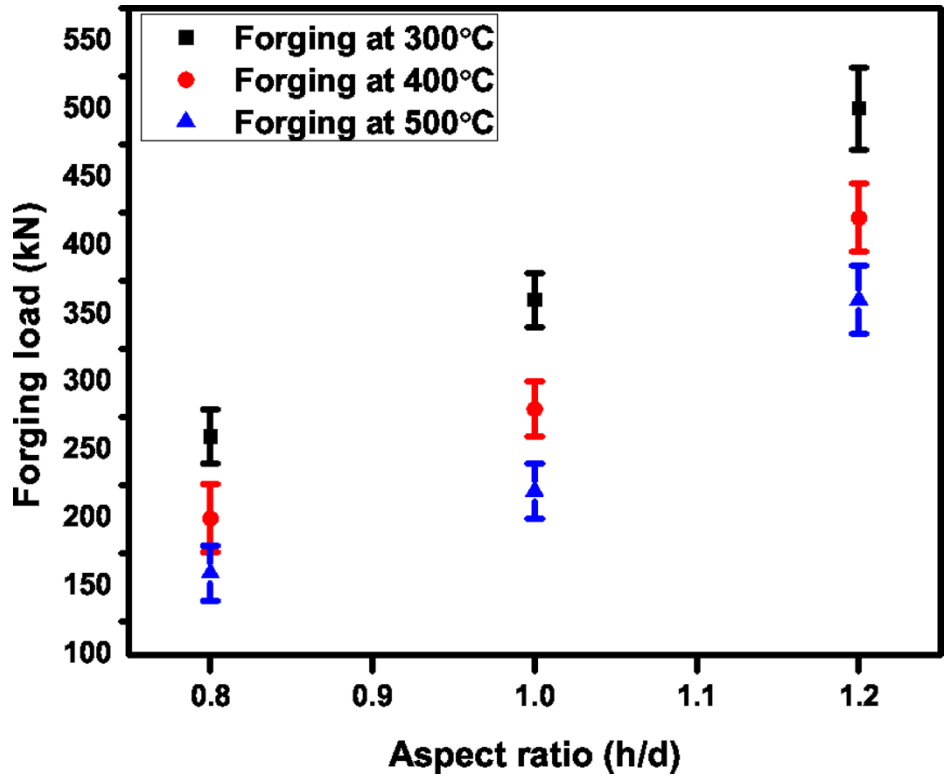

Figure 3.11 Variation of forging load with aspect ratio (h/d) at different working temperatures under unlubricated condition

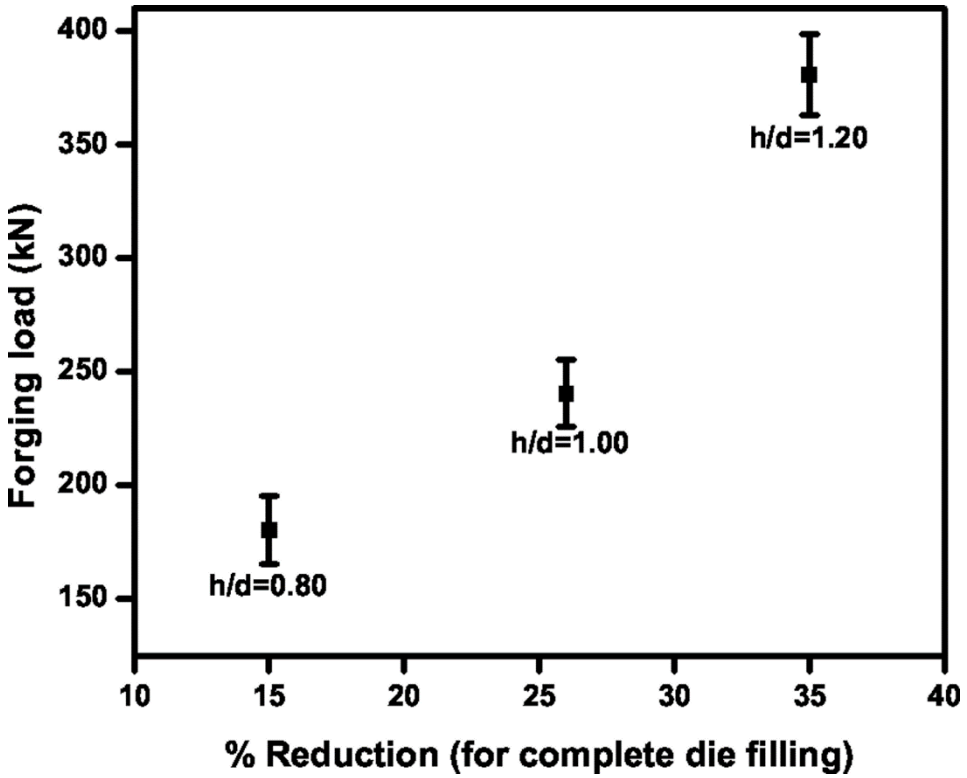

Figure 3.12 Variation of forging load with percentage reduction in height for different aspect ratios during impression die forging at 400°C under lubricated condition

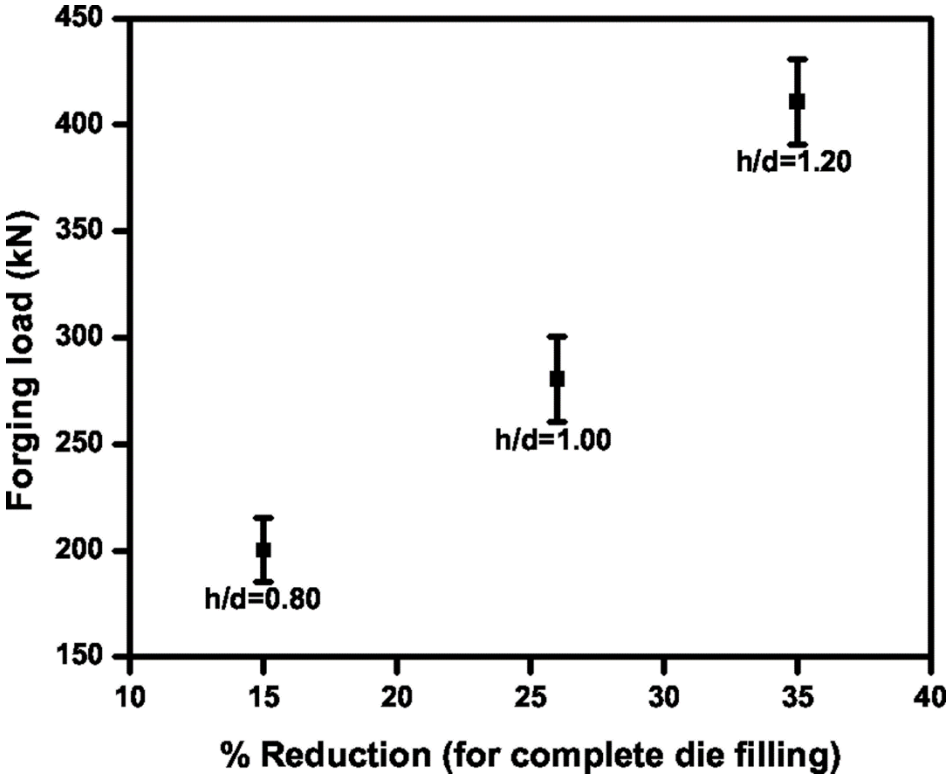

Figure 3.13 Variation of forging load with percentage reduction in height for different aspect ratios during impression die forging at 400°C under unlubricated condition

Figures 3.12 and 3.13 show the variation of forging load with percentage reduction in height for different aspect ratios during impression die forging at 400°C under lubricated and unlubricated conditions. The results show that the test sample with h/d=1.20 requires the highest forging load to fill the die impression with 35% reduction in height in both lubrication conditions as compared to other aspect ratios. Under lubrication, due to the relatively low coefficient of friction test samples require relatively less forging load as compared to the unlubricated condition in all aspect ratio.

Figure 3.14 shows the forging load plotted against percentage reduction in height during impression die forging of the alloy. During the initial part of the compression (portion 'ABC' for unlubricated and 'abc' for lubricated condition), the breakdown of coarse silicon and intermetallic particles take place and in turn refined and highly oriented structure developed. However, with an increase in forging load, the test sample starts to generate surface cracks from stress concentration sites between silicon-intermetallic

particles and Al matrix. These cracks gradually propagate at the circumferential surface of the test samples. During compression, the lubricated sample showed more movement of the circumferential surface as compared to unlubricated one (Narayanasamy et al., 2008).

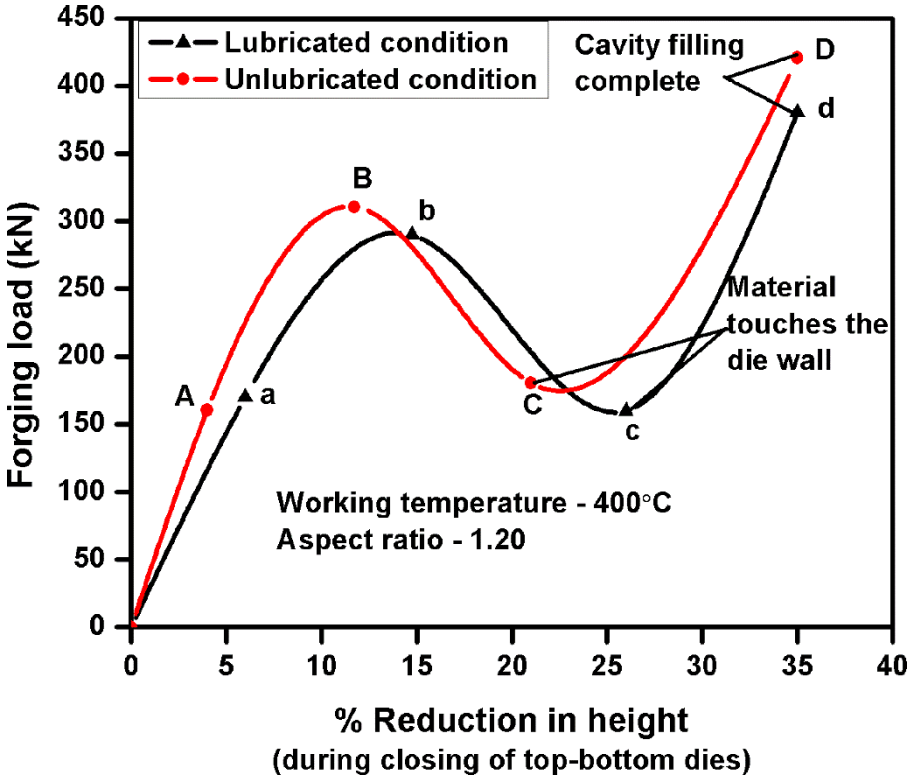

Figure 3.14 Forging load plotted against percentage reduction in height for complete die closing under lubricated and unlubricated conditions

Now, due to bulging the test sample comes in contact of the die walls (point C for unlubricated and c for lubricated condition) and upon further loading, the lateral spread continues till the sample fills the die cavity completely (point D for unlubricated and d for lubricated condition). The lubricated condition shows relatively less forging load and more lateral spread than the unlubricated condition.

The above results reveal that bulk processing of the complex hypereutectic Al-18Si-2.5Cu-0.6Fe alloy through impression die forging was feasible and produces defect free forged products. The successful processing of such complex alloy through impression die forging was encouraged to authors to investigate the bulk processing of the alloy through

the converging section. Therefore, converging die forging of the above alloy was conducted to investigate the deformation behavior under various processing conditions.

3.2.2.4 Deformation behavior of the complex hypereutectic Al-Si alloy during forging through the converging die

Converging die forging of the complex hypereutectic Al-18Si-2.5Cu-0.6Fe was performed using billets with reduction ratios of 1.5 and 2.0 at elevated temperatures. Figures 3.15(a-c) shows the three regimes of Si particles and intermetallic phase distribution with Al matrix during the hot forging of hypereutectic Al-Si alloy through a converging die.

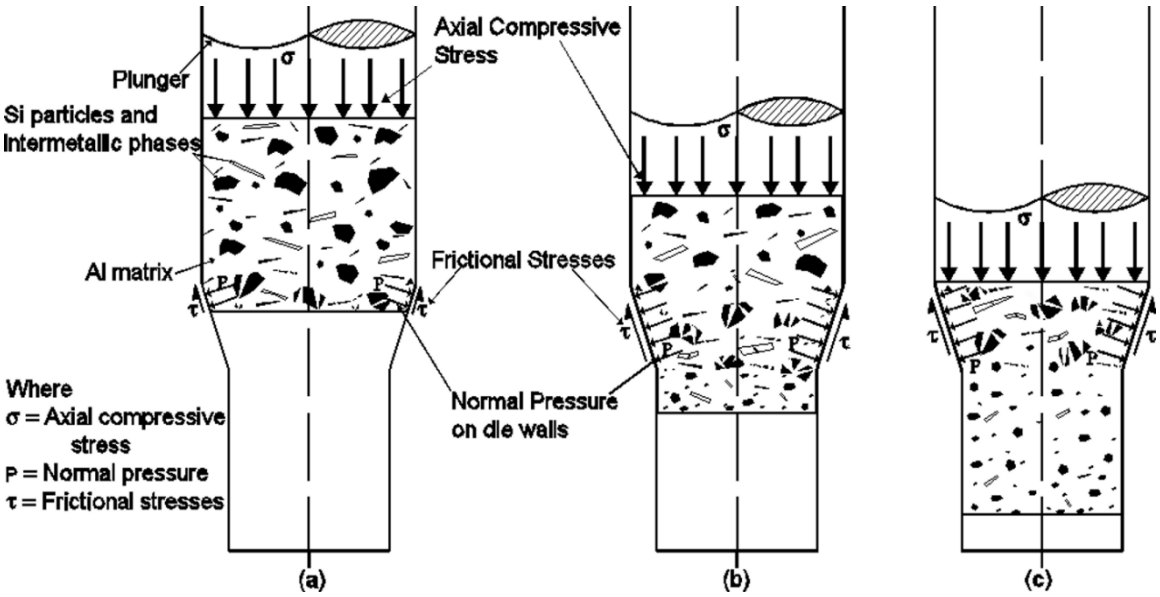

Figure 3.15 Three regimes of Si particles and intermetallic phase distribution with Al matrix during forging of complex hypereutectic Al-Si alloy through converging die

During high-speed forging of the alloy through converging die at elevated temperatures, huge axial compressive stresses were exerted on the billet along with severe friction between the contacting surface of die wall and the billet as shown in Figure 3.15(a). Due to the axial stress, there was heavy deformation and the consequent flow of the billet through converging section of the die which caused the breakdown of the coarse silicon and the intermetallic compounds into fine particles to consequently reform strong Al-Si structure. Thus, in this process, the soft aluminum matrix deformed plastically whereas

the blocky primary and eutectic silicon particles got fractured and fragmented, and consequently distributed more uniformly in the matrix (Figures 3.15(b-c)). Since a significant amount of heat being generated between contacting die wall and billet surface during the process of compression, therefore graphite lubricant was used to reduce the frictional effect.

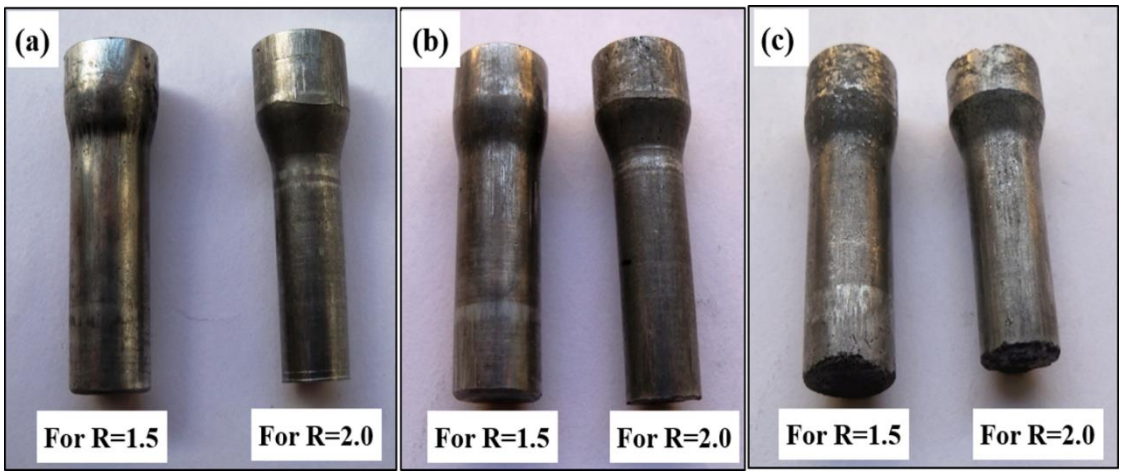

Figure 3.16 Photographs of forged products at various elevated working temperatures (a) 300°C, (b) 400°C, and (c) 500°C

Figures 3.16(a-c) show the photograph of forged samples under different processing conditions. It is evident from the results that the samples forged at 300°C (Figure 3.16(a)) shows much better surface finish than 500°C (Figure 3.16(c)) processing temperature. This is due to the fact that at higher processing temperature (500°C) the fractured and fragmented silicon-intermetallic particles have a tendency to flow outwards circumference along with plastically deformed Al matrix. It is also evident that the test samples forged at a low reduction ratio (R=1.50) show better surface finish as compared to the one with higher reduction ratio (R=2.0). It may due to higher reduction ratio causes severe friction between contacting surfaces during compression, and thus reduces the surface finish of the deformed billet. Figure 3.17 show forging load plotted against working temperatures for different reduction ratio (R) during converging die forging. The results reveal that higher deformation load required to compress the material at low

working temperature for all reduction ratio and it decreases with increasing the working temperature. Since the alloy contains a large amount of the hard silicon particles and intermetallic compounds which in turn decreases the formability of the alloy. At higher working temperature, the thermal softening of the Al matrix takes place which results in formability of the alloy increases and consequently decreases the deformation load, while the hard Si particles remain undeformed at this working temperature. Therefore, the Al matrix is deformed at hot processing condition while the hard silicon particles get fragmented during the process.

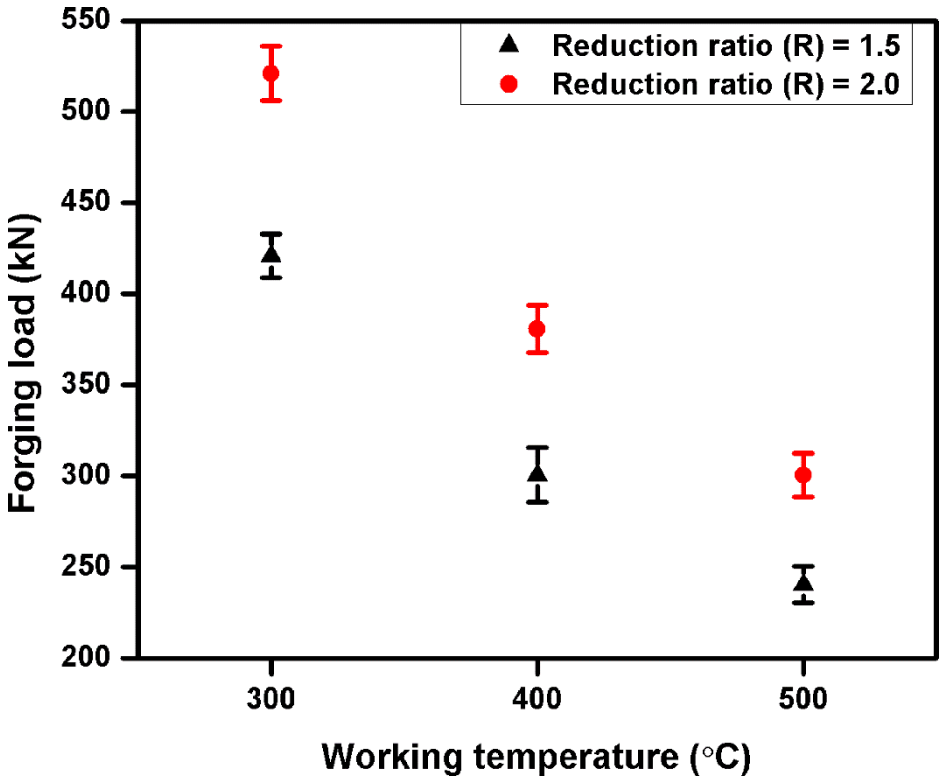

Figure 3.17 Forging load plotted against working temperatures for different reduction ratios

3.2.3 Microstructural features of forged complex hypereutectic Al-18Si-2.5Cu-0.6Fe alloy

Microstructural studies of the forged alloy were carried out to study the effect of bulk processing on grain morphology and their distribution in the matrix. The detailed experimental procedures were discussed in section 2.6.

Figures 3.18-3.20 shows the optical micrograph of the forged samples with the aspect ratio (h/d) of 1.20, 1.00, and 0.80 at 300°C, 400°C, and 500°C working temperatures under lubricated and unlubricated conditions respectively. The average grain size of the primary and eutectic silicon particles observed under different processing conditions was listed in Tables 3.1 and 3.2.

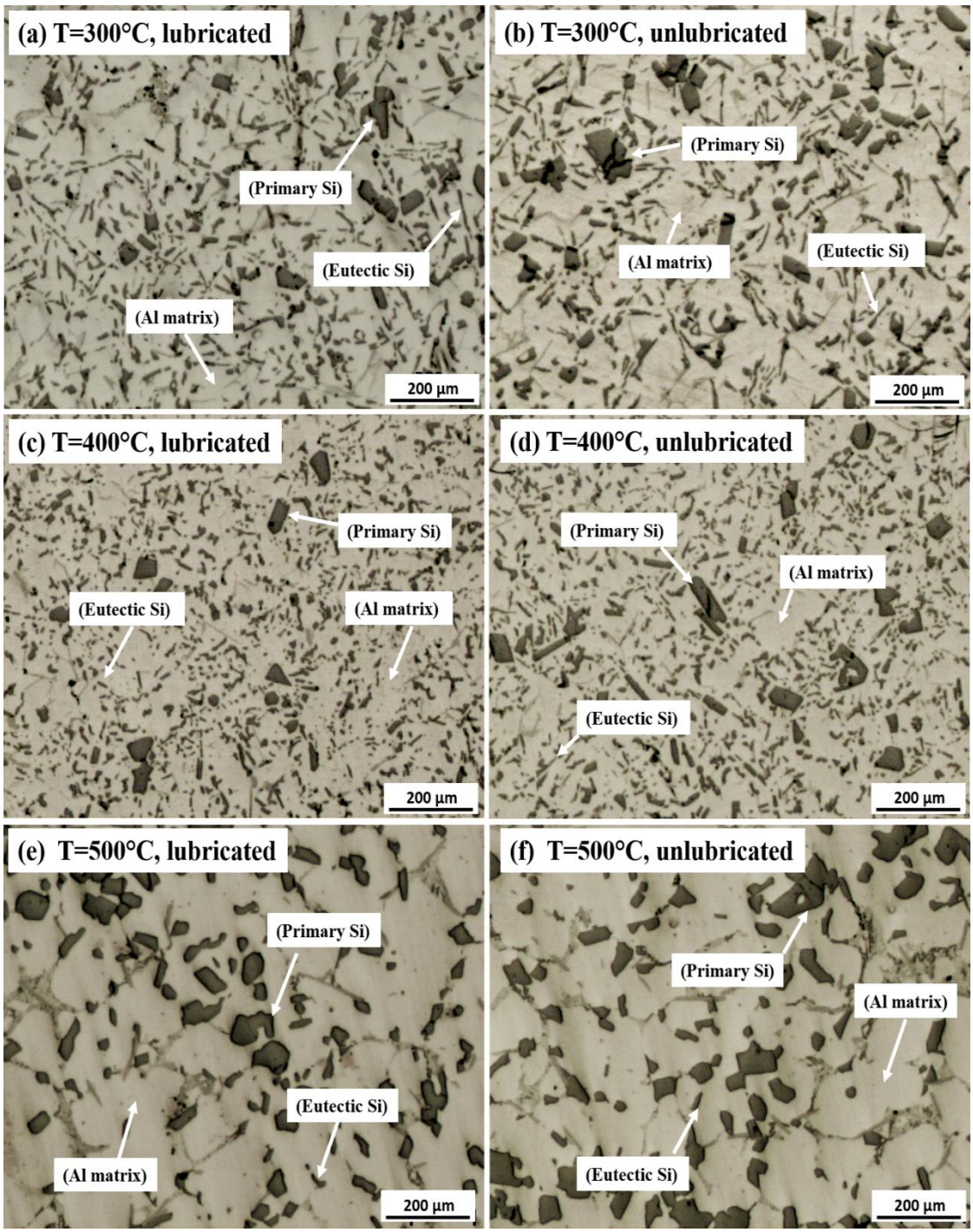

Figure 3.18 Optical microstructure of the forged samples at aspect ratio 1.20 under lubricated and unlubricated conditions

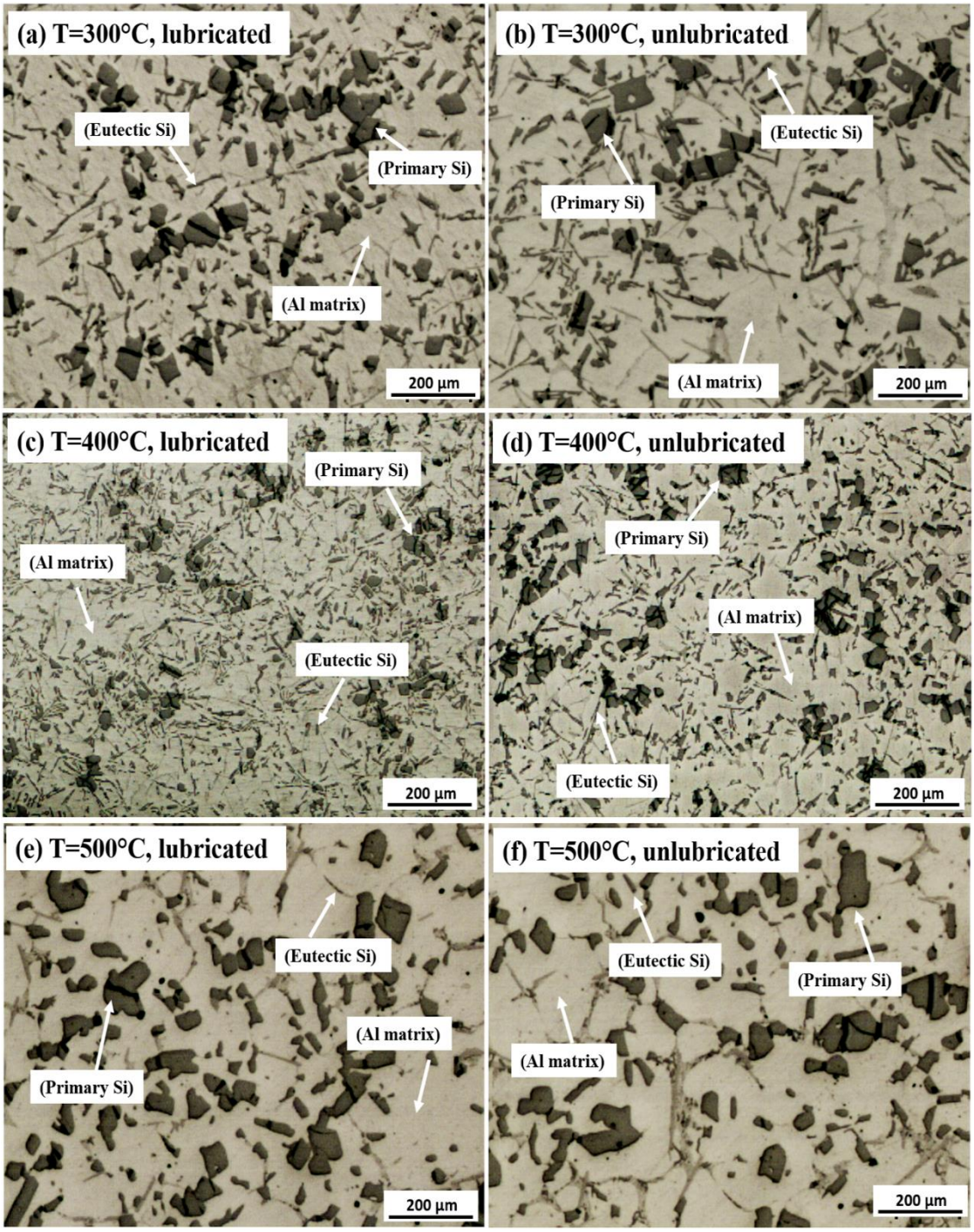

Figure 3.19 Optical microstructure of the forged samples at aspect ratio 1.0 under lubricated and unlubricated conditions

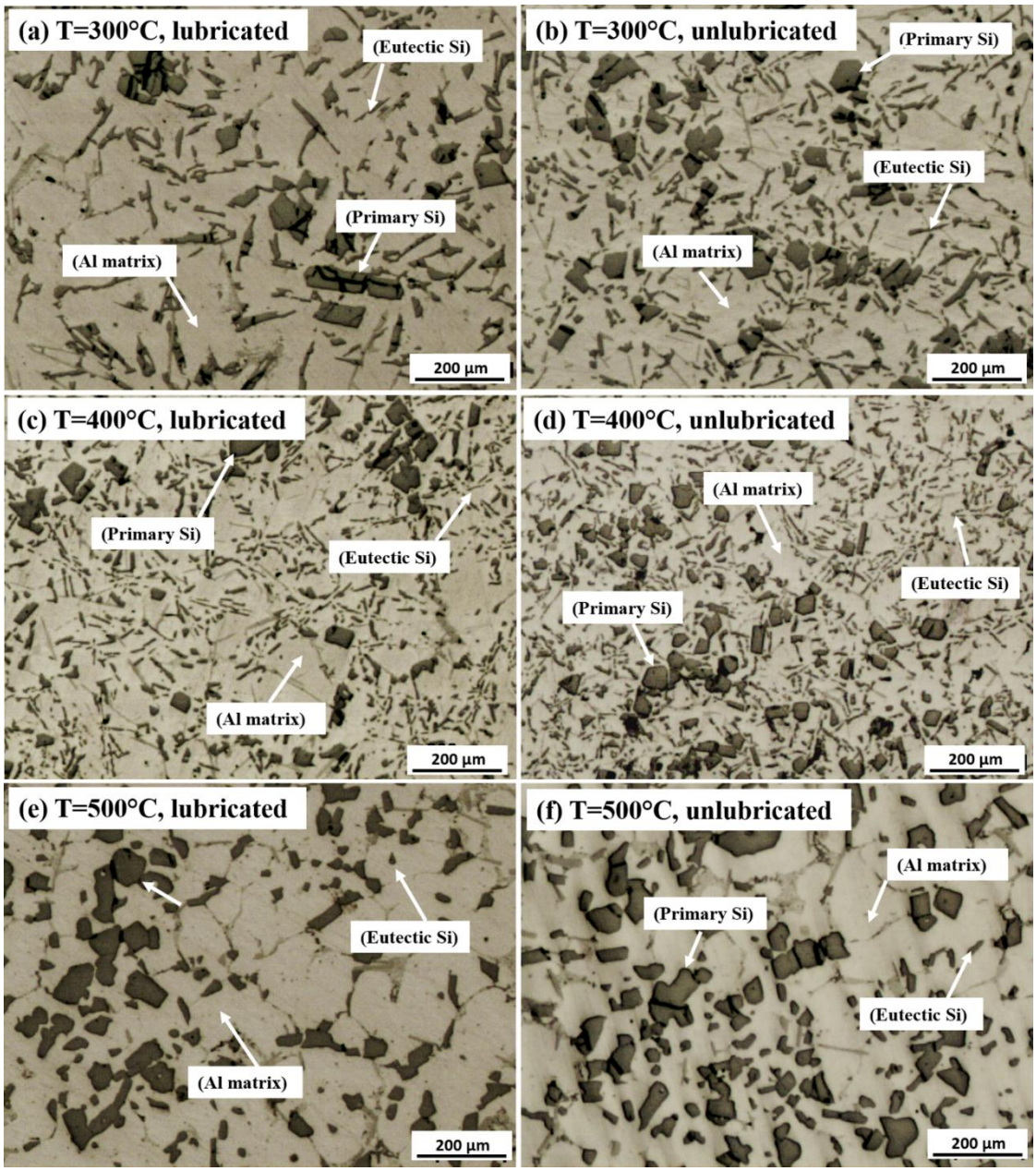

Figure 3.20 Optical microstructure of the forged samples at aspect ratio 0.80 under lubricated and unlubricated conditions

Table 3.1 Variation of average grain size of the primary silicon particle in forged samples under different processing conditions

Aspect Ratio (h/d)	Mean diameter/Standard deviation of the primary Si particles under different forging temperatures (µm)					
	300°C		400°C		500°C	
	Lub. cond.	Unlub. cond.	Lub. cond.	Unlub. cond.	Lub. cond.	Unlub. cond.
1.20	22.6/11.2	23.7/16.8	17.9/16.8	19.5/17.8	30.1/20.7	33.3/22.2
1.00	26.9/17.8	30.2/20.7	19.5/10.1	20.9/10.5	32.3/25.6	35.1/25.4
0.80	28.8/14.9	27.1/18.1	20.7/18.8	22.2/16.2	33.3/17.1	36.2/24.5

Table 3.2 Variation of average grain size of the eutectic silicon particle in forged samples under different processing conditions

Aspect Ratio (h/d)	Mean diameter/Standard deviation of eutectic Si particle under different forging temperatures (μm)					
	300°C		400°C		500°C	
	Lub. cond.	Unlub. cond.	Lub. cond.	Unlub. cond.	Lub. cond.	Unlub. cond.
1.2	16.6/8.2	20.1/10.2	11.6/8.5	13.6/8.8	23.2/9.5	19.9/7.7
1	22.2/7.7	26.3/14.5	15.5/12.9	15.4/10.6	23.2/9.6	23.7/16.8
0.8	21.8/17.3	22.4/14.5	22.9/13.3	16.7/12.1	25.6/10.4	26.1/12.7

The Figures 3.21(a-f) show optical micrographs of the forged billet with reduction ratio R= 1.5 and 2.0 at 300, 400 and 500°C working temperatures. Table 3.3 shows the average grain size of the primary and eutectic silicon particles in the samples forged at different working temperatures of 300, 400 and 500°C, and reduction ratios of 1.5 and 2.0.

Table 3.3 Average grain size Si particles in forged samples at different processing temperatures

Forging temperature (°C)	Primary Si particles size at different reduction ratio (R)				Eutectic Si particles size at different reduction ratio (R)			
	R=1.5		R=2		R=1.5		R=2	
	Mean dia. (μm)	Stand. dev. (μm)	Mean dia. (μm)	Stand. Dev. (μm)	Mean dia. (μm)	Stand. Dev. (μm)	Mean dia. (μm)	Stand. Dev. (μm)
300	13.1	4.8	10.3	3.7	10.4	3.7	8.9	3.5
400	10.1	3.5	7.5	3.1	8.4	3.2	6.7	2.8
500	17.1	5.7	13.4	5.5	5.6	3.0	6.5	3.1

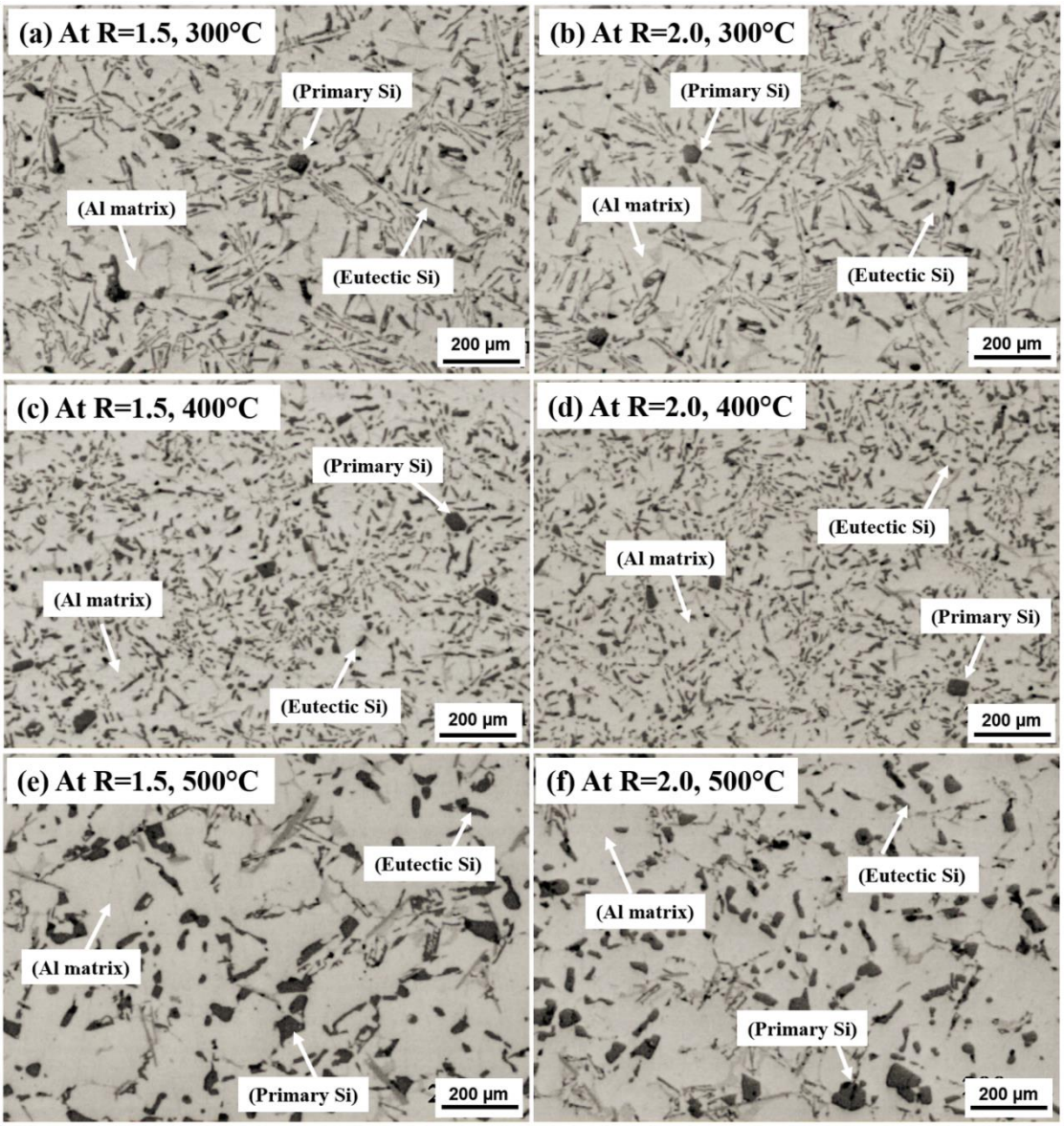

Figure 3.21 Optical micrographs of the forged billets (a) R=1.5, T=300°C, (b) R=2.0, T=300°C, (c) R=1.5, T=400°C, (d) R=2.0, T=400°C, (e) R=1.5, T=500°C, and (f) R=2.0, T=500°C

The microstructural refinement is noticed in both impression die and converging die forging of the complex alloy at elevated temperatures of 300, 400, and 500°C. Since alloy was bulk processed through pre-set working temperatures of 300, 400, and 500°C, in both die setups. Therefore, the refinement phenomenon of the forged alloy at such processing temperatures of 300, 400, and 500°C were was quite similar to impression die forging. However, the extent of microstructural refinement was greater in converging die forging due to severe deformation of the alloy during processing through the converging section.

The alloy was soaked at the pre-set working temperatures of 300, 400, and 500°C for approximately one hour for compositional homogenization prior to deformation. During this period as well during the process of deformation there would have been precipitation of elemental silicon and intermetallic compounds containing Cu, and Fe giving rise to finer precipitates of Si and the intermetallic compounds. In addition, several coarse particles undergo high speed of deformation during compressive loading. The hard and brittle silicon-intermetallic particles could not sustain the applied load, got fragmented, and uniformly distributed along with laterally flowing soft aluminum matrix. As a result, microstructural refinement was observed with fine particles of Si and the intermetallics in the forged samples (Figures 3.18-3.21). The degree of fragmentation depends on the stress level applied to the sample, orientation of the particle, and its size.

The results show that the degree of refinement increased with increase in the working temperature from 300 to 400°C (Tables 3.1, 3.2, and 3.3) because of decrease in the yield strength and consequent increase in bulk deformation of the material. However, an increase in the working temperature from 400 to 500°C led to coarsening of the silicon particles (Figures 3.18-3.21(e-f)) due to the faster rate of diffusion. The fragmentation and subsequent distribution in the matrix depend on the working temperatures, aspect ratios or reduction ratios.

Results from Tables 3.1 and 3.2 in impression die forging, it is evident that at 400°C working temperature, 1.20 aspect ratio and lubricated interfacial conditions produce fine particles. The degree of fragmentation depends on the stress level applied to the sample, orientation of the particle, and its size. The complete separation of the particles in the form of fragments could be observed at 200 kN and temperature around 300°C. The tendency to round off the fragmented particles where indicated in the microstructure of the samples deformed at relatively high temperature whereas irregular shape was the characteristics of the low-temperature deformation.

The results also show that Lubricated conditions show much better grain refinement. The refinement in microstructure is observed which gradually improves for aspect ratio 1.20 as compared with 1.00 and 0.80.

The processing at 400°C was found to be optimum in terms of the distribution and fine size of the second phase particles as well refinement of the grains of the matrix during converging die forging. It may be attributed to the relatively higher degree of plastic deformation than that of 300°C and a lower rate of diffusion than that of 500°C. In addition, the microstructural refinement of the forged alloy was more significant at high reduction ratio R=2.0 during converging compression in all the working conditions.

The results form Table 3.1 and 3.2 clearly indicates that refinement in Si grain was almost the same in both lubricated conditions, and very slight variation in their size. The working temperature of 300°C is found to be relatively low whereas 500°C is the relatively high working temperature for bulk deformation. The existing studies by various investigators have also reported a similar trend during different processing techniques of other Al-Si alloys. They have found that silicon particles get fragmented due to deformation load and uniformly dispersed in the Al matrix (Baiqing et al., 2003; Cui et al., 2010). Haghdadi et al., 2012 reported the coarsening of Si particles at the higher processing temperature.

3.2.4 Mechanical properties of the forged complex hypereutectic Al-18Si-2.5Cu-0.6Fe alloy

3.2.4.1 Tensile strength of the forged alloy

Tensile tests were conducted to study the effect of various process parameters on the tensile strength of the material during bulk processing. Literature by various authors reveal that processing parameter such as aspect ratio or reduction ratio and working temperature deformation significantly affect the tensile strength of the forged alloy. Therefore, the tensile test was done, and the detailed experimental procedures were discussed in section 2.7. The ultimate tensile strength (UTS) of the as-cast alloy was

found to be 115±6 MPa. Figures 3.22-3.24 show the engineering stress-strain curves of the as-cast and forged samples (lubricated conditions) with aspect ratios (R) 1.20, 1.00 and 0.80 at 300, 400 and 500°C working temperatures.

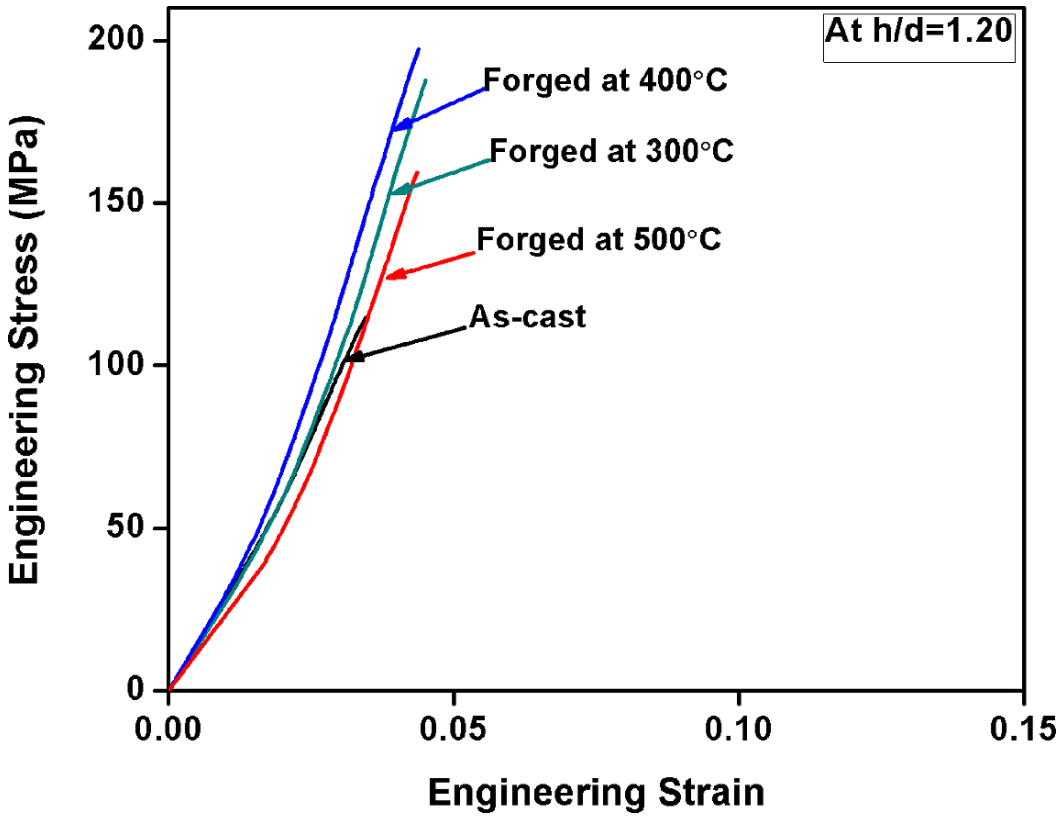

Figure 3.22 Stress-strain diagrams of the as-cast and forged samples (h/d=1.20)

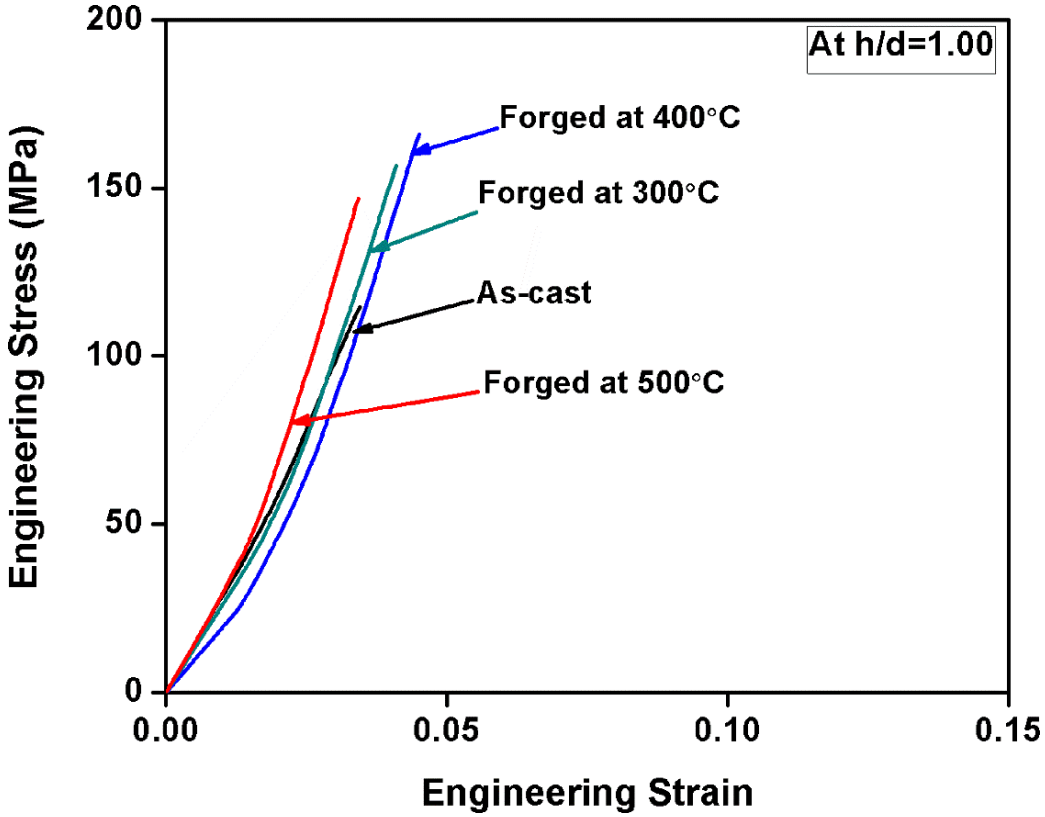

Figure 3.23 Stress-strain diagrams of the as-cast and forged samples (h/d=1.00)

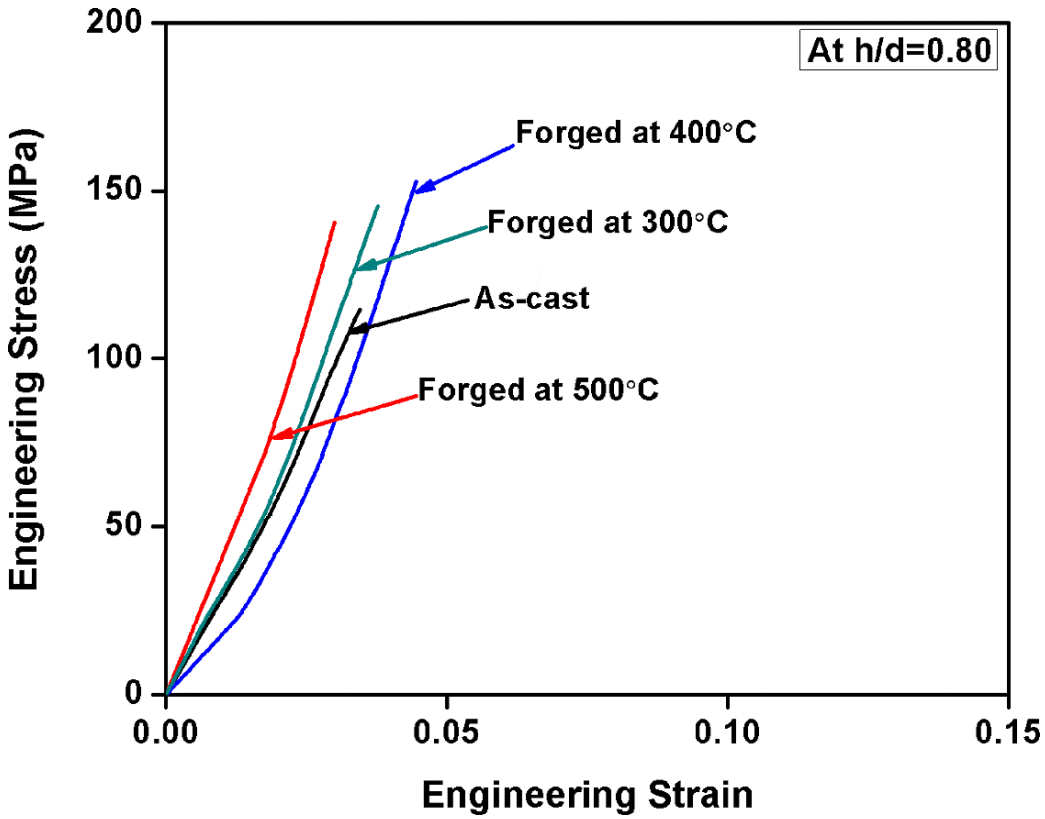

Figure 3.24 Stress-strain diagrams of the as-cast and forged samples (h/d=0.80)

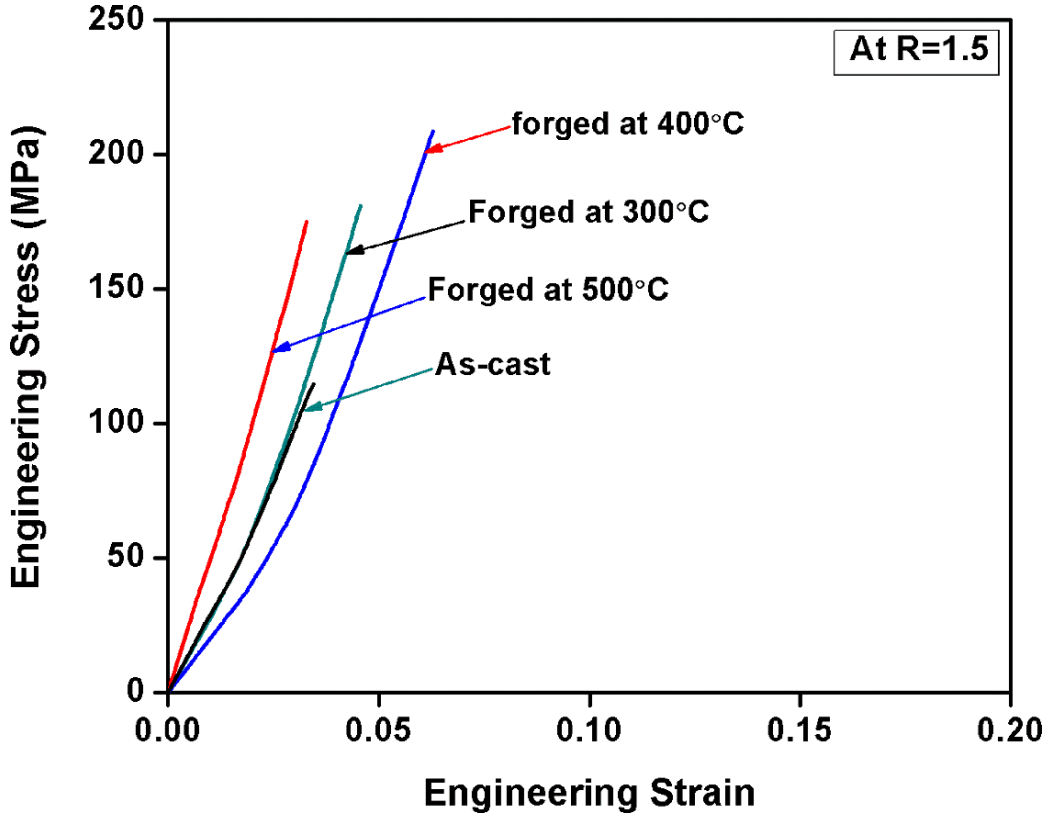

Figure 3.25 Stress-strain diagrams of the as-cast and forged samples (R=1.5)

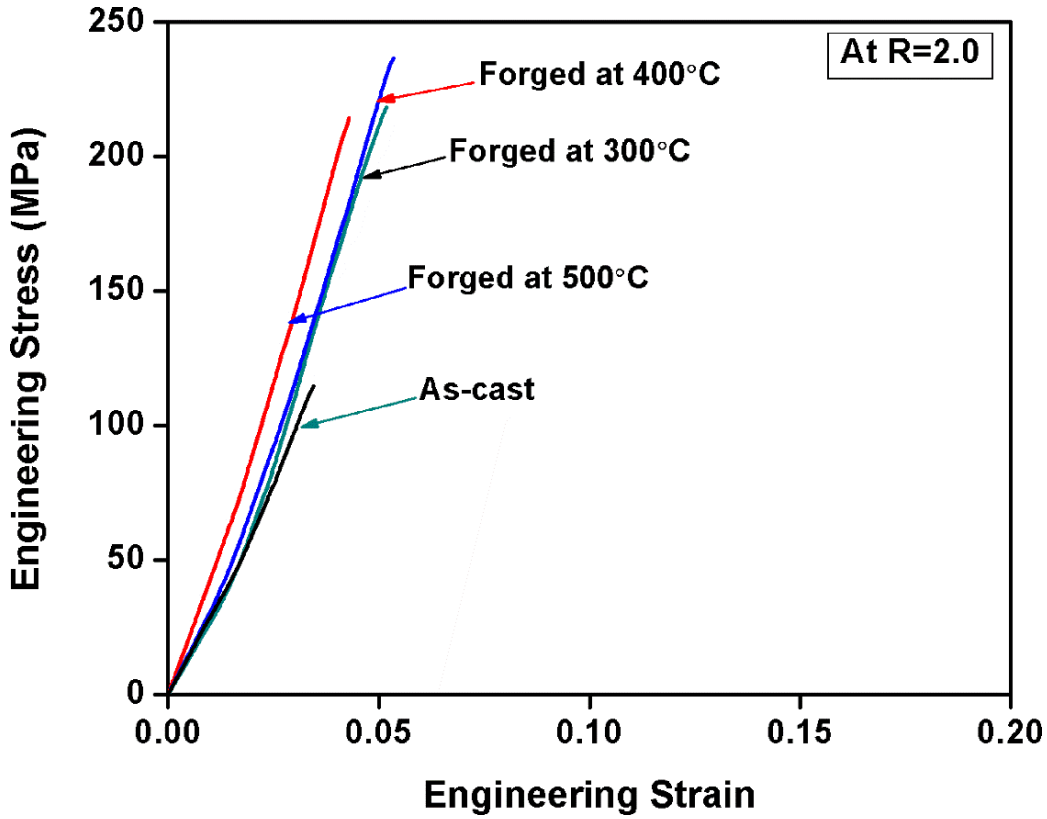

Figure 3.26 Stress-strain diagrams of the as-cast and forged samples (R=2.0)

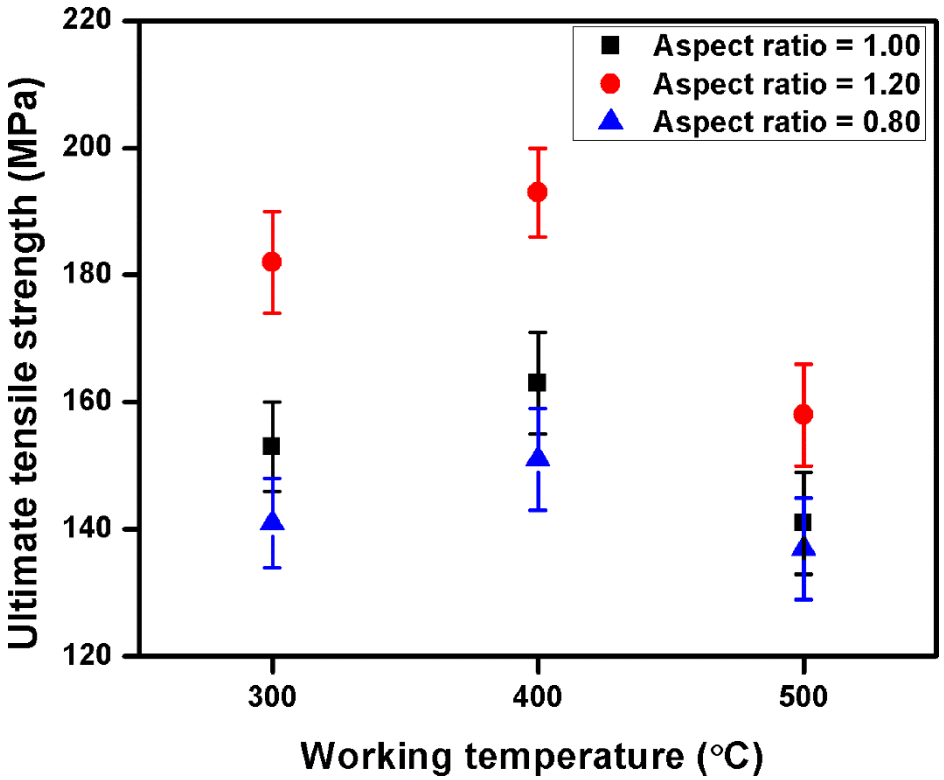

Figure 3.27 Ultimate tensile strength (UTS) of the forged samples shown against different h/d ratios and working temperatures (°C) under lubricated condition

Figures 3.25 and 3.26 show the engineering stress-strain curves of the as-cast and forged samples with reduction ratios (R) 1.5 and 2.0 at 300, 400 and 500°C working temperatures. The UTS of the forged alloy through impression die under various processing conditions as shown in Figure 3.27. The results show that significant improvement in tensile strength of the forged alloy in both die conditions. The forged alloy through converging die also shows similar tensile behavior as the alloy bulk processed through impression die. However, tensile strength was slightly higher for samples forged through the converging die. It may be due to refinement in microstructural features were slightly higher which in turn enhances the tensile strength of the forged alloy through converging die.

It may be seen that there was a brittle fracture in all the cases without any plastic deformation in both impression and converging die conditions. The yield strength is usually taken as the stress corresponding to 0.2% plastic strain. It is evident from the

Figures 3.22-3.26 that there was almost no plastic deformation; the deformation was essentially elastic in nature; therefore only the ultimate tensile strength is shown. The tensile behavior of the alloy Al-18Si-2.5Cu-0.6Fe (wt.%) in the present investigation as seen to be similar to that of the alloy Al-20Si-1.5Fe-0.6Mn (wt.%) shown in Figure 4(c) of the earlier investigation by Suárez-Rosales et al., 2016. The brittle behavior of that alloy was attributed to the presence of iron to form the brittle intermetallic compound of iron with a strength less than that of even silicon. Thus, the brittle fracture during the tensile test of the Al-18Si-2.5Cu-0.6Fe (wt.%) alloy in the present investigation may be attributed to the formation of iron-rich intermetallic compounds. There is a significant improvement in tensile strength of the forged samples in all the processing conditions as shown in Figures 3.22-3.26. It may be attributed to strong bonding between the fragmented second phase fine particles and grain refinement of the Al matrix as per the Hall-Petch strengthening mechanism (Ma et al., 2016). The decrement in strength from compression at the high working temperature of 500°C resulted from coarsening of Si atoms due to the faster rate of diffusion and also grain growth of the matrix. Also in the literature, fine size silicon particles have been reported to contribute to the strengthening of the alloys (Mallapur et al., 2011; Wu et al., 2014). Reduction in tensile strength due to coarsening of the microstructure at higher processing temperatures has been reported also earlier (Shaha et al., 2014).

The tensile strength of the impression die product with h/d=1.2 and forged at 400°C under lubricated conditions indicate the best results (Figure 3.22). Aspect ratio significantly affects the UTS of the forged alloy as shown in Figure 3.27. It is attributed to the percentage reduction in height which is higher for the samples with aspect ratio 1.20 (35%) as compared to others 1.0 (26%) and 0.80 (15%) and thus cause significant deformation of the alloy. Such deformation generates a high density of dislocation and

also refines the microstructure which leads to considerable improvement in UTS of the forged alloy.

The results also reveal that the alloy forged at higher reduction ratio (R=2.0) possess higher tensile strength due to greater microstructural refinement during processing (Figure 3.26).

3.2.4.2 Hardness

Hardness tests were conducted to study the effect of various process parameters on the hardness value of the material during bulk processing. Therefore, the hardness test was done, and the detailed experimental procedures were discussed in section 2.7. The hardness of the as-cast was found to be 78±3 HV.

Figures 3.28 and 3.29 show the hardness value of the forged alloy through impression die and converging die, respectively.

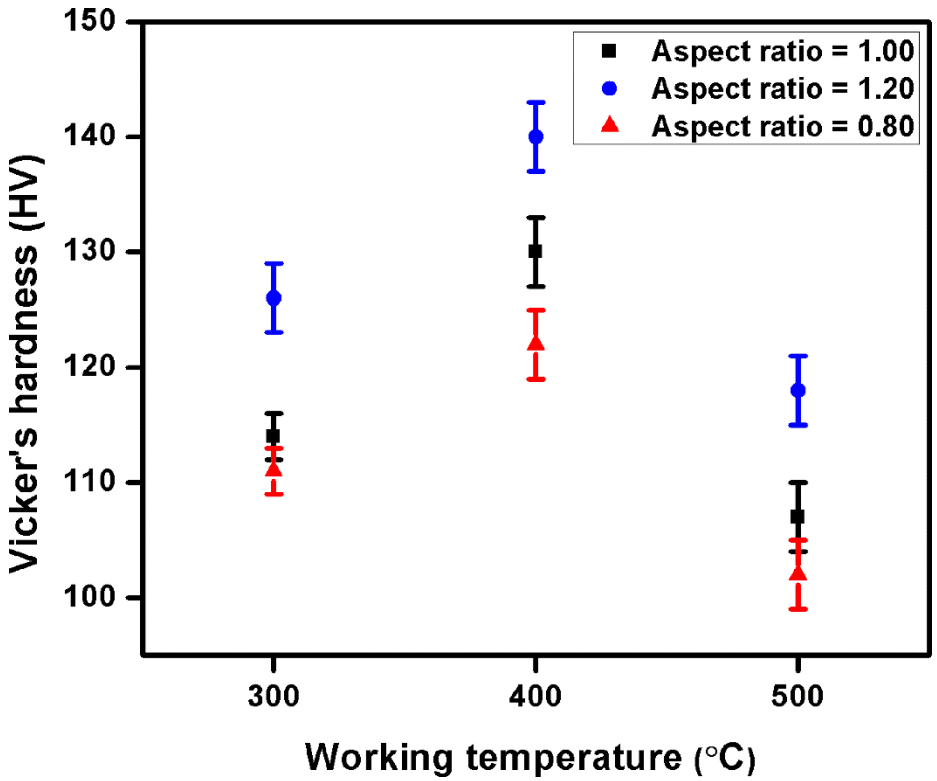

Figure 3.28 Vicker's microhardness of the forged samples shown against different h/d ratios and forging temperatures (°C) under lubricated condition

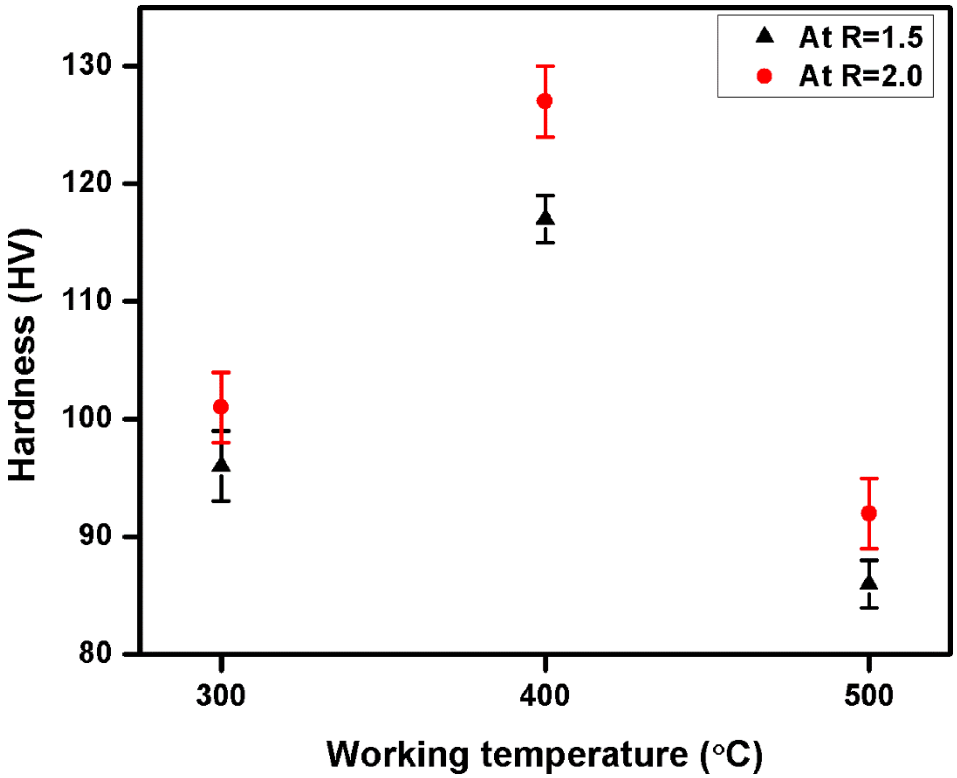

Figure 3.29 Vicker's microhardness of the samples forged to different reduction ratios (R) of 1.5 and 2.0 at different forging temperatures

The significant improvement observed in the hardness of the forged alloy as compared with as-cast alloy during bulk processing. The improvement phenomenon in hardness value of the forged alloy was similar in both the impression and converging die forging. It may be due to the same processing temperatures 300, 400 and 500°C were applied during processing. Therefore, almost similar results were obtained during hardness test. The strengthening mechanisms mentioned in section 3.2.4.1 also explain the observed increase in the hardness from compression at elevated temperatures (Figures 3.28 and 3.29). The hardness was relatively higher for the samples forged at 400°C as compared to the other working temperatures of 300 and 500°C for all aspect and reduction ratios. The decrease in hardness from compression at 500°C is essentially due to coarsening of the second phase particles and also the coarsening of grains of the matrix. The relatively lower hardness from processing at 300°C in respect of that at 400°C may be related to less refinement of the second phase particles at 300°C.

From these results, it is seen that hardness of the alloy depends mainly on the microstructural characteristics of the forged alloy. The improvement in the hardness of the forged alloy may be attributed to an increase in dislocation density during compression at high strain rate and more uniform dispersion of the second phase particles in the Al matrix. Various investigators have also reported a similar trend during the processing of other complex Al-Si alloys through different techniques. They have confirmed that microstructural refinement and higher dislocation density enhanced the hardness of the alloy (Jamaati et al., 2011; Rajabi et al., 2009).

3.2.4.3 Fractography

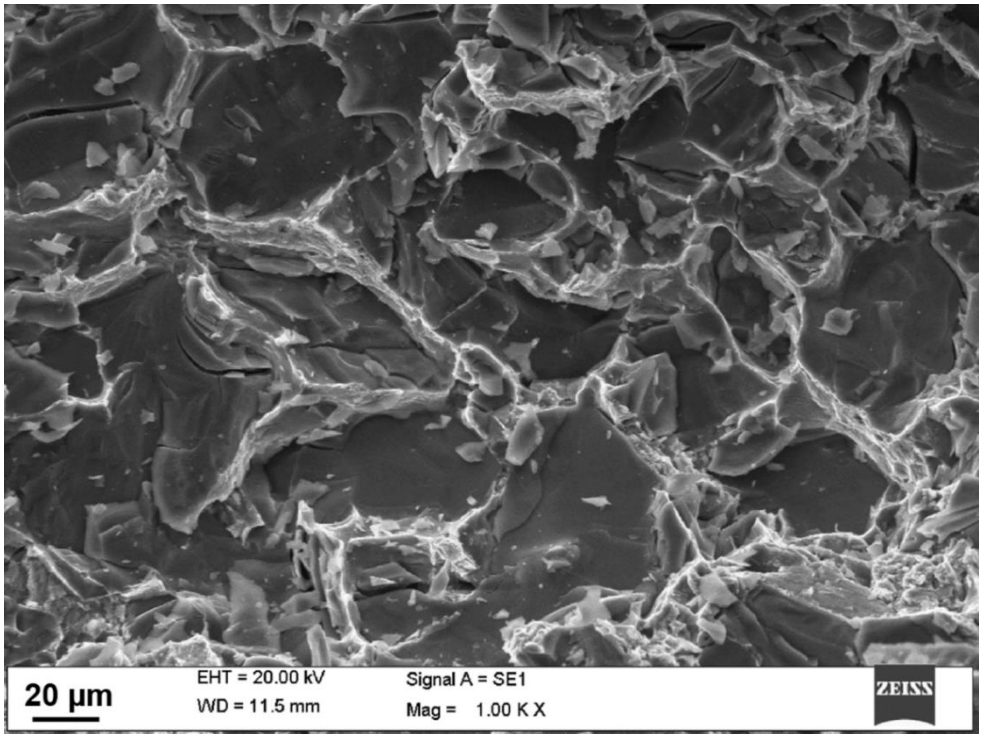

Figure 3.30 SEM image of the as-cast tensile fractured surface

Figure 3.30 shows SEM micrograph the tensile fracture surface of the as-cast alloy. The fracture morphology of as-cast alloy shows brittle failure indicates a fracture of primary silicon particles with very less or negligible plastic deformations of the alloy. It occurred due to the presence of hard silicon and intermetallic particles with almost insignificant ductility and failed without plastic deformation (Figure 3.30). It is attributed to the

initiation of stress concentration between the Al matrix and coarse primary silicon-intermetallic particles while microvoids are formed near the needle-shaped eutectic silicon during the straining process. As a result of this, cracks initiate and propagate along with these particles and Al matrix.

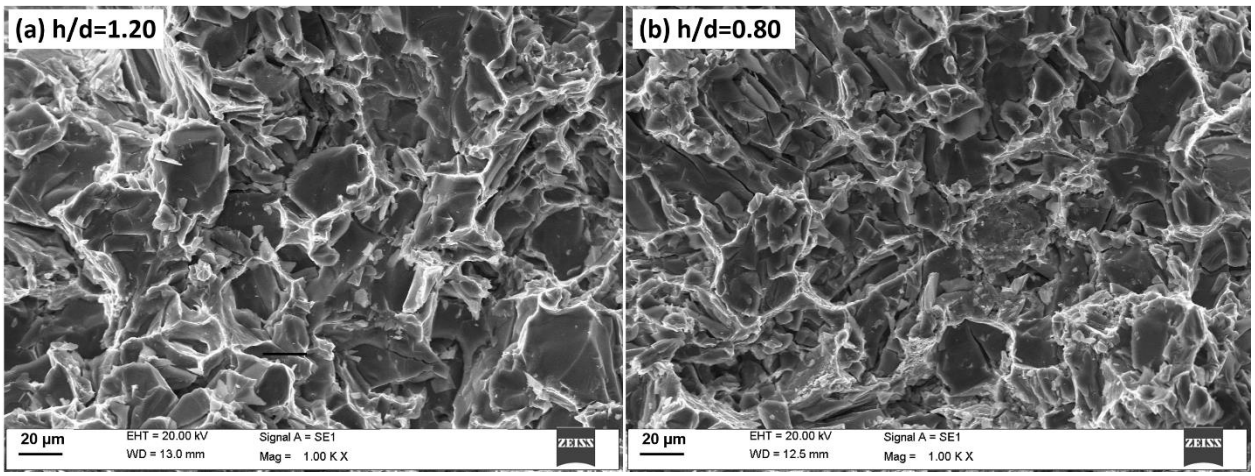

Figure 3.31 SEM images of the fractured surface at 400°C working temperature for aspect ratios (a) 1.20 and (b) 0.80

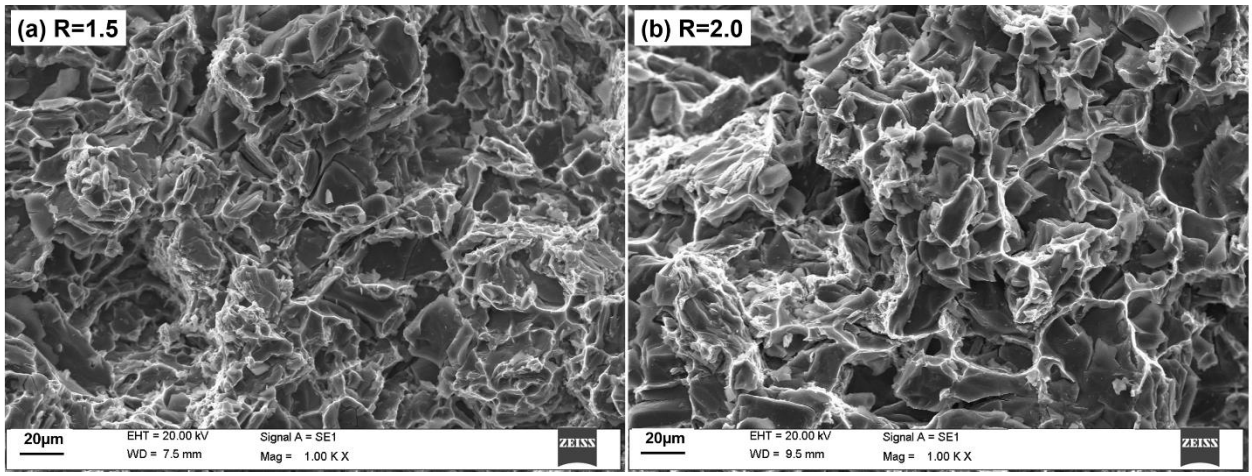

Figure 3.32 SEM images of the fractured surface of the samples forged at 400°C and reduction ratios (a) R=1.50, and (b) R=2.0

Figures 3.31(a), and 3.31(b) show the fractured surface of the samples forged at 400°C with 1.20 and 0.8 aspect ratio under lubricated conditions. While Figures 3.32(a) and 3.32(b) shows the tensile fractured surface of the deformed samples with reduction ratios of 1.50 and 2.0 and forged at 400°C. The fracture morphology indicates brittle failure of the test samples in both forging conditions. The strength of the alloy improved during

bulk processing in both die conditions with the expense ductility, and the material failed during straining without necking. Thus, to achieve higher tensile strength and avoid the premature failure of the alloy it is recommended to reduce the silicon particles size and improved grain structure.

Previous studies on various complex Al-Si alloys processed through different other techniques also support the results of the present investigation. It was found that coarse Si particles and their non-uniform dispersion are responsible for the failure of the alloys. It may due to high stress concentration developed between coarse Si particles and Al matrix during loading, generates micro-cracks with further propagating and grow until the failure during straining (Cui et al., 2010; Mallapur et al., 2011).

3.2.5 Wear behavior of the as-cast and forged complex hypereutectic Al-18Si-2.5Cu-0.6Fe alloy

Dry sliding wear test was conducted to investigate the effect of bulk processing on the wear performance of the complex Al-18Si-2.5Cu-0.6Fe alloy. Different process parameters such as percentage reduction, deformation rate, and working temperatures involved during bulk processing which significantly affect the wear behavior of the processed alloy. Therefore, proper selection of such process parameters significantly enhances the wear resistance of the processed alloy. However, wear resistance of the material depends on the hardness value and its higher the alloy with greater hardness value. Past studies by various investigators also confirmed that the material with higher hardness value shows a low wear rate (Xu et al., 2007).

The results reveal that hardness of the forged alloy considerably improved in both the die setups as compared with as-cast alloy as discussed in the previous section 3.2.4.2. The results also reveal that the hardness value of the forged alloy is almost same in both the die setups, thus their wear behavior may be similar under the same test conditions. However, the improvement in the microstructural features and tensile strength of the

material are better in converging die forging as compared with impression die. Therefore, wear test of forged samples in converging die was conducted, and the detailed experimental procedures were discussed in section 2.8

3.2.5.1 Wear behavior of the as-cast and forged complex hypereutectic Al-Si alloy through converging die

Figures 3.33 and 3.34 show the variation in cumulative weight loss with sliding distance (SD) of the as-cast and forged samples with R=1.5 and 2.0 at applied normal load 20 N. It indicates that the cumulative weight loss increases with increasing sliding distance for all the test samples. It was also observed that the test sample forged at 400°C shows the least cumulative weight loss among all the test samples.

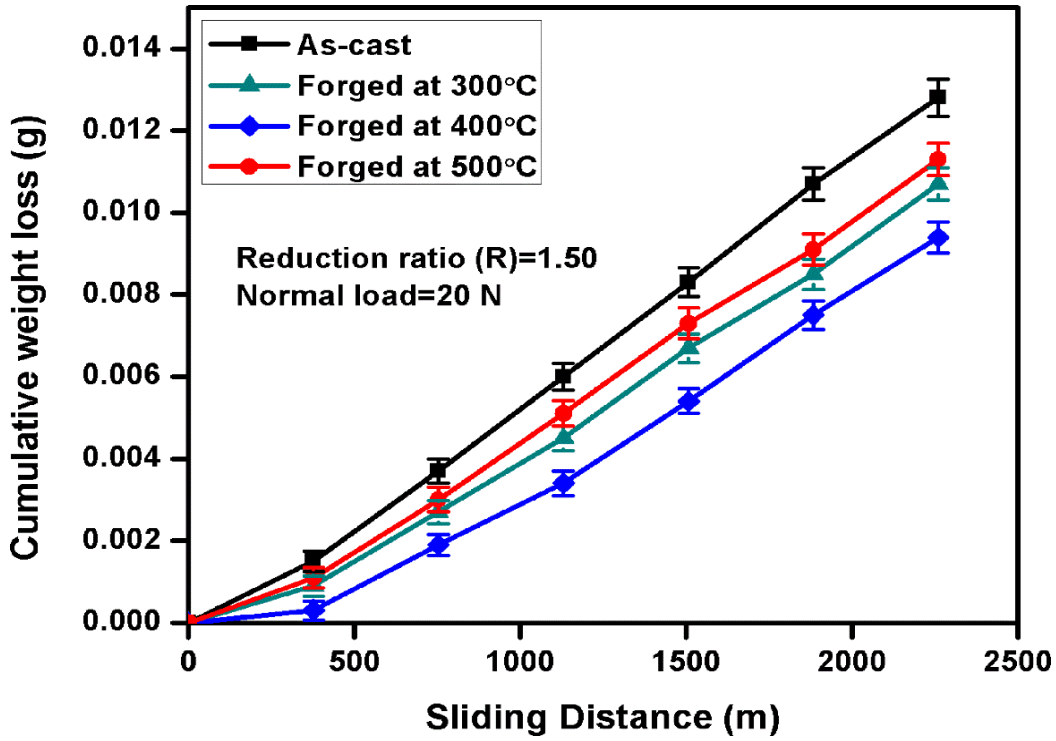

Figure 3.33 Cumulative weight loss of the as-cast and forged samples (R=1.5) under different conditions

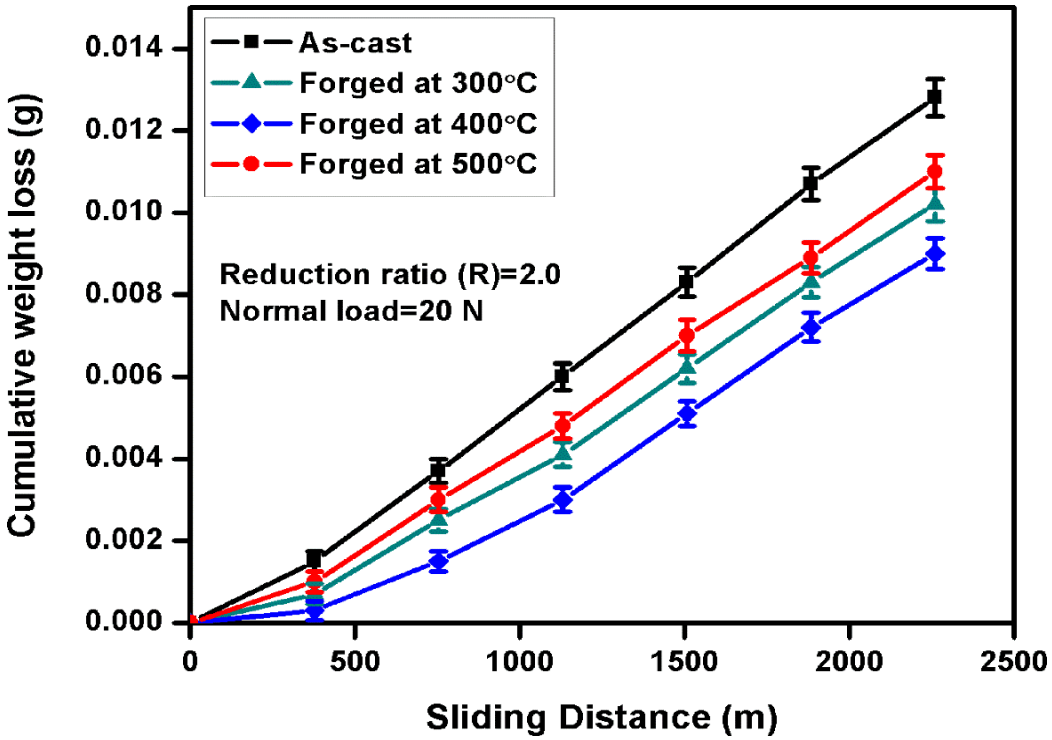

Figure 3.34 Cumulative weight loss of the as-cast and forged samples (R=2.0) under different conditions

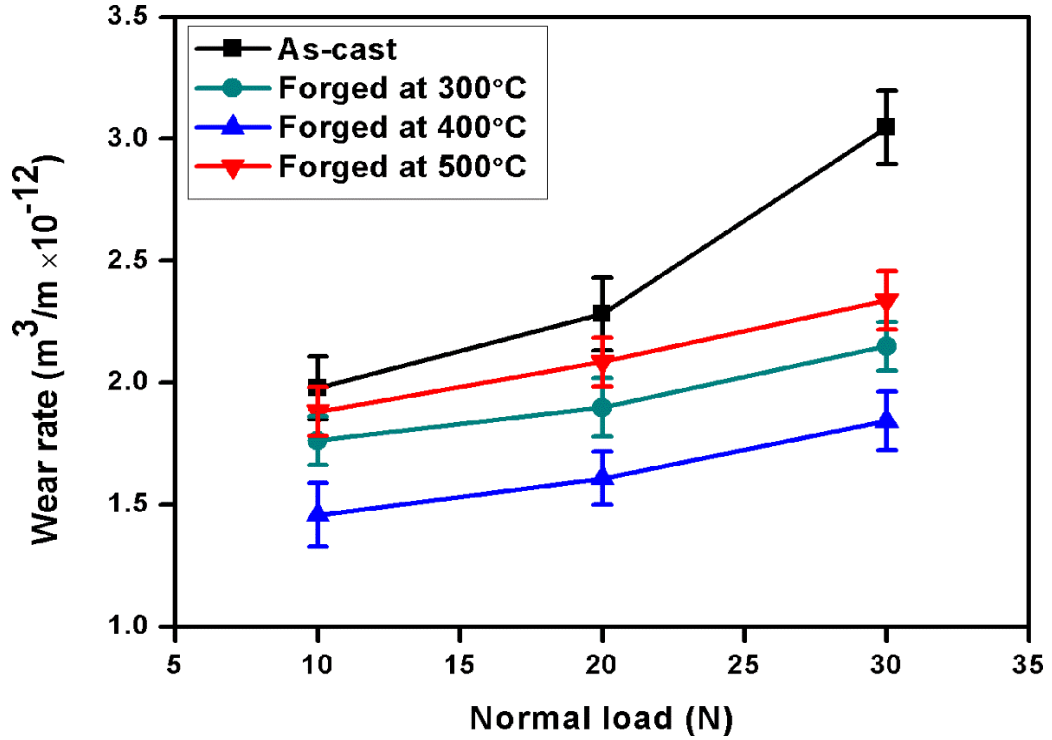

Figure 3.35 Wear rate of the as-cast and forged samples at R=1.5 and 10, 20, 30 N normal loads

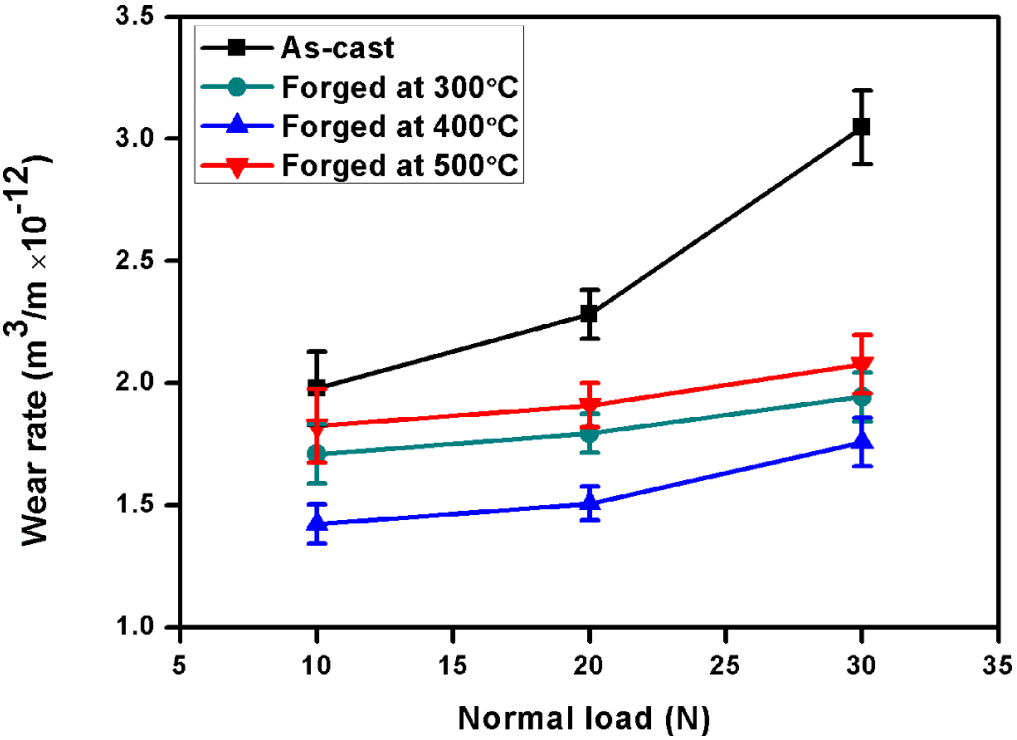

Figure 3.36 Wear rate of the as-cast and forged samples at R=2.0 and 10, 20, 30 N normal loads

Figures 3.35 and 3.36 show the variation of wear rate with the applied normal load for the as-cast and forged samples respectively, at sliding distance of 2260 m, sliding velocity 1.3 m/s, and working temperatures 300, 400 and 500°C for reduction ratios R=1.5 and 2.0. It was observed that for the as-cast alloy initially the wear rate increases slowly with applied normal load up to 20 N, thereafter increases sharply on further increase in the load, whereas it increases slowly in the forged test sample as shown in Figure 3.35. The lowest wear rate was observed for the sample forged at 400°C. However, the as-cast alloy exhibits the highest wear rate. Similar variation in wear rate against applied normal load was also observed with the reduction ratio of 2.0 as shown in Figure 3.36. The results also indicate that wear resistance of the forged alloy increases with an increase in reduction ratio in all the test conditions.

Wear rate of the forged samples decreased with increase in working temperature during compression from 300-400°C, and a reverse trend started with the further increase in the processing temperature from 400-500°C as shown in Figures 3.35 and 3.36, respectively.

Further, minimum wear rate is observed at 400°C for both the reduction ratios, which indicates that the forged alloy gives a better tribological performance at this working temperature. The similar tribological trend was also observed by various researchers for other Al-Si alloys (Lozano et al., 2009; Srivastava and Ojha, 2004).

3.2.5.2 Wear Mechanism

Figures 3.37 and 3.38 depict the worn surface morphology of the as-cast and forged samples.

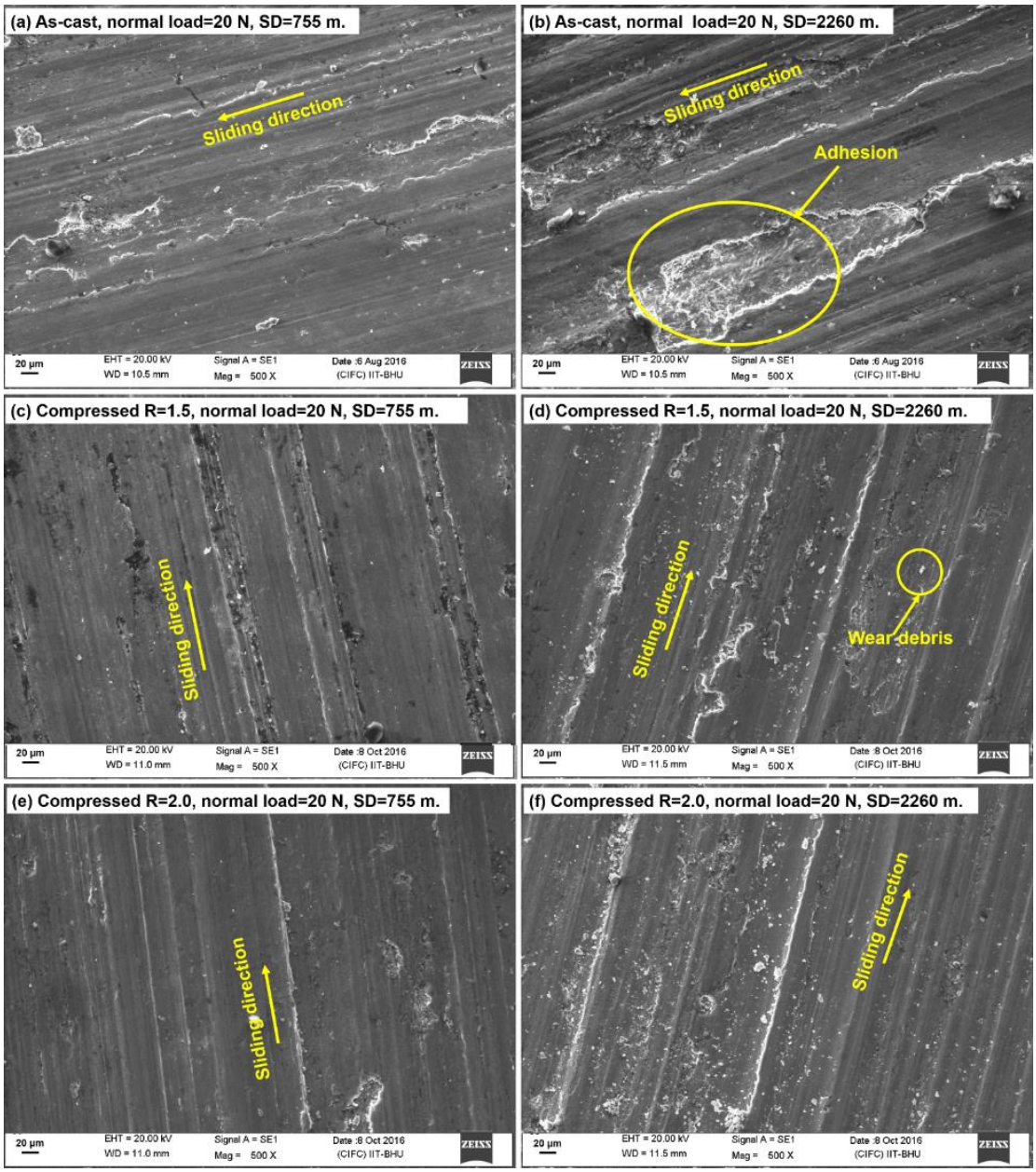

Figure 3.37 Worn surface morphology of the as-cast and sample forged at 400°C, at constant applied normal load of 20 N, sliding velocity of 1.3 m /s for different sliding distances

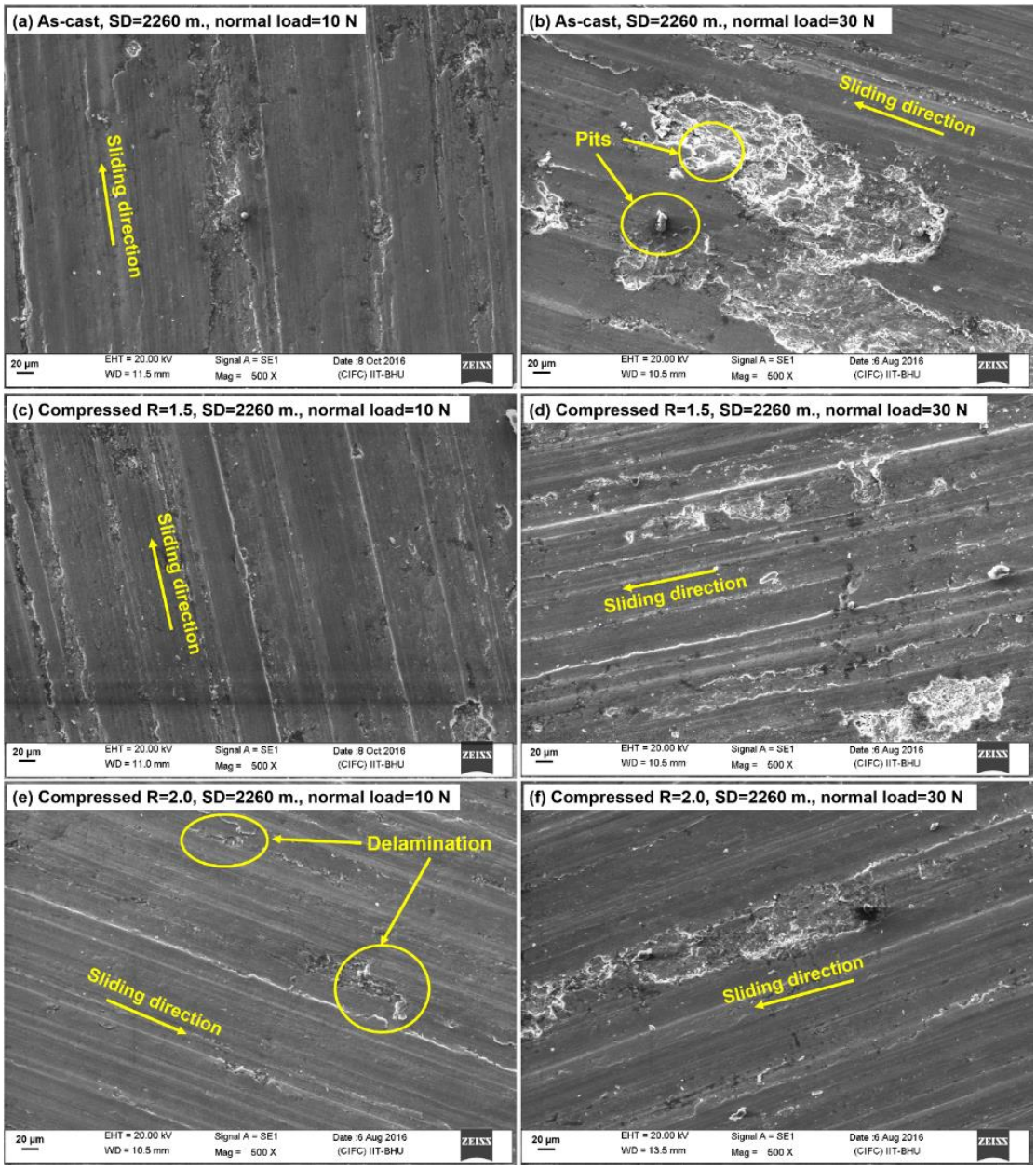

Figure 3.38 Worn surface morphology of the as-cast and samples forged at 400°C, at constant sliding distance of 2260 m, sliding velocity of 1.3 m /s for different applied normal loads

Wear resistance of the Al-Si alloy depends on the morphology and distribution of hard silicon particles, intermetallic compounds in Al matrix and the hardness of the alloy (Raghukiran and Kumar, 2013; Sharma and Dwivedi, 2005). The present study speculates that the wear resistance of the alloy in the as-cast condition was poor as compared to the forged samples. Figure 3.39 depicts the EDS spectrum of the worn surface of the forged alloy (R=2.0 at 400°C) at 30 N normal load and sliding distance of 2260 m. It can be

observed from the EDS spectrum of the worn surfaces that no additional compound formed during the rubbing of the interacting surfaces.

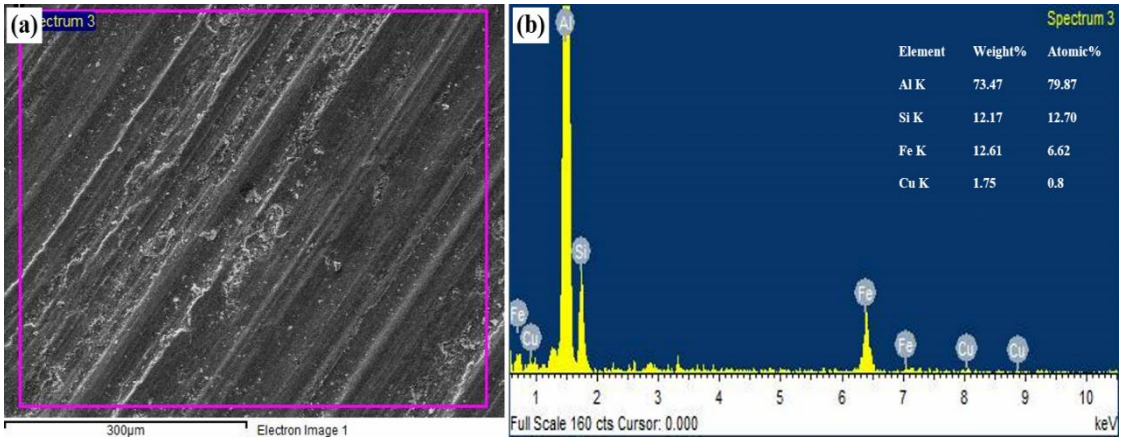

Figure 3.39 SEM micrograph of the worn surface of the sample forged at R=2.0 and 400°C (a) at 30 N normal load and sliding distance 2260 m, and (b) corresponding EDS analysis

Figures 3.37(a-f) show the worn surface morphology of the as-cast and forged samples (R=1.5 and 2.0 at 400°C) at constant normal load (20 N) and sliding speed of 1.3 m/s for different sliding distances (SD=755 and 2260 m). It may be observed from Figures 3.37(a-f) that as the sliding distance increases, worn surface morphology changes from mild to severe wear. From Figures 3.37(a-f), it is clear that adhesion and abrasion were the primary wear mechanisms involved in the material during dry sliding. Adhesive wear increases as the sliding distance increase probably, due to a higher localized frictional heat produced during the sliding, which led to softening of the alloy, and consequent increase in the adhesion. Grooves, trench, and scratches like morphology were also observed, probably caused by abrasion. However, the grooves were wider and deeper when the sliding distance (SD) is 2260 m as compared to 755 m. It also attributes to softening of the alloy due to higher localized frictional heating during sliding. Due to softening, the resistance to the penetration of asperities of the counter surface became lower, thus hard asperities penetrated deeply. The resistance to abrasion increases as the reduction ratio increases, as seen in Figures 3.37(a-f). It is attributed to the increase in

hardness with an increase in reduction ratio. On the contrary, the adhesion decreases in forged samples as the reduction ratio increases, as shown in Figures 3.37(c-f).

Wear debris containing hard Si particles were also observed as shown in Figure 3.37(a)-(f). Si particles are being ejected from the subsurface by repeated flexion in one direction. Poor worn surface morphology of the as-cast alloy was observed as compared with the forged samples with an increase in sliding distance. A similar trend was also reported earlier that increase in sliding distance generates severe friction between the contacting pin and the counter disc, which results in high wear of the alloy and consequently produces severely worn surface morphology (Kucukomeroglu, 2010).

Figure 3.38(a-f) shows the worn surface morphology of the as-cast alloy and the forged samples (R=1.5, 2.0 and 400°C) at constant sliding distance SD=2260 m and sliding speed of 1.3 m/s for different applied normal loads of 10 and 30 N. It was also observed that as the load increases, worn surface morphology becomes more severe (Figure 3.38). It reflects that abrasion and adhesion phenomena dominate with the increase in load. In other words, as the normal load increases, penetration of hard steel counter asperities into the soft aluminum alloy surfaces increases, which deforms the soft aluminum matrix plastically. It produces a bulk amount of material loss, i.e. increase in wear rate of the alloy at a higher normal load. In addition, several hard Si particles squeeze out at higher applied loads, which act as a third body abrasion between the pin and counter surfaces which also contribute to enhancing the wear rate. Also, the increase in adhesion was more as compared to abrasion as can be confirmed by the formation of pits as shown in Figure 3.38(b). With increasing load, the increase in abrasion can be attributed to the deeper penetration of asperities of the counter surface while adhesion increased due to an increase in braking energy. Increase in braking energy led to increased heat accumulation at the interacting surfaces which led to plastic deformation of the alloy. This plastic deformation tends to weld the alloy with the counter surface which causes an increase in

adhesion. As the reduction ratio increases, abrasion and adhesion both decrease. At reduction ratio R=2.0, some delamination was also observed; and the crater developed by delamination was small as compared to the crater developed by adhesion. No significant delamination was observed at R=1.5. Abrasion and adhesion, both increase with an increase in load in the as-cast alloy and forged alloy with R=1.5. In contrast, for reduction ratio 2.0, abrasion behavior did not change much with an increase in load, however adhesion increased significantly. This can be attributed to the increased hardness for R=2.0. Earlier studies have also shown a similar trend during wear testing of other complex Al-Si alloys (Alshmri et al., 2014; Vijeesh and Prabhu, 2014).

3.2.5.3 Roughness measurement

Figure 3.40 shows the three dimensional AFM roughness morphology and their respective roughness profiles of the worn surfaces of the as-cast and forged alloy with reduction ratios (R) 1.5 and 2.0 for the scanning area of 50 µm × 50 µm for each sample.

The worn surfaces of different samples were produced under a normal load of 20 N and sliding velocity of 1.3 m/s using a pin-on-disc machine. The AFM morphology of the worn surface of the as-cast alloy which reveals that root mean square (rms) roughness (Rq) was found to be 0.503 µm as shown in Figure 3.40(a). However, Rq of worn surface of the forged sample with reduction ratios 1.5 and 2.0 was found to be 0.347 and 0.277 µm respectively as shown in Figures 3.40(b) and (c). It is very clear from the AFM results that the Rq of the forged sample with R=1.5 and 2.0 was much lower compared to the as-cast alloy. It reflects the low wear of the forged materials during dry sliding because of their higher hardness as compared to that of the as-cast alloy, which obeys the Archard's law (Chen et al., 2005). The Rq was also decreased with an increase in reduction ratio (Figure 3.40). The depth of penetration was very high (≈1270 nm) in case of the as-cast sample as shown in Figure 3.40(a). However, the depth of penetration in the forged

sample with reduction ratios 1.5 and 2.0 was reduced significantly to ≈950 and ≈730 nm respectively as shown in Figures 3.40(b) and 3.40(c).

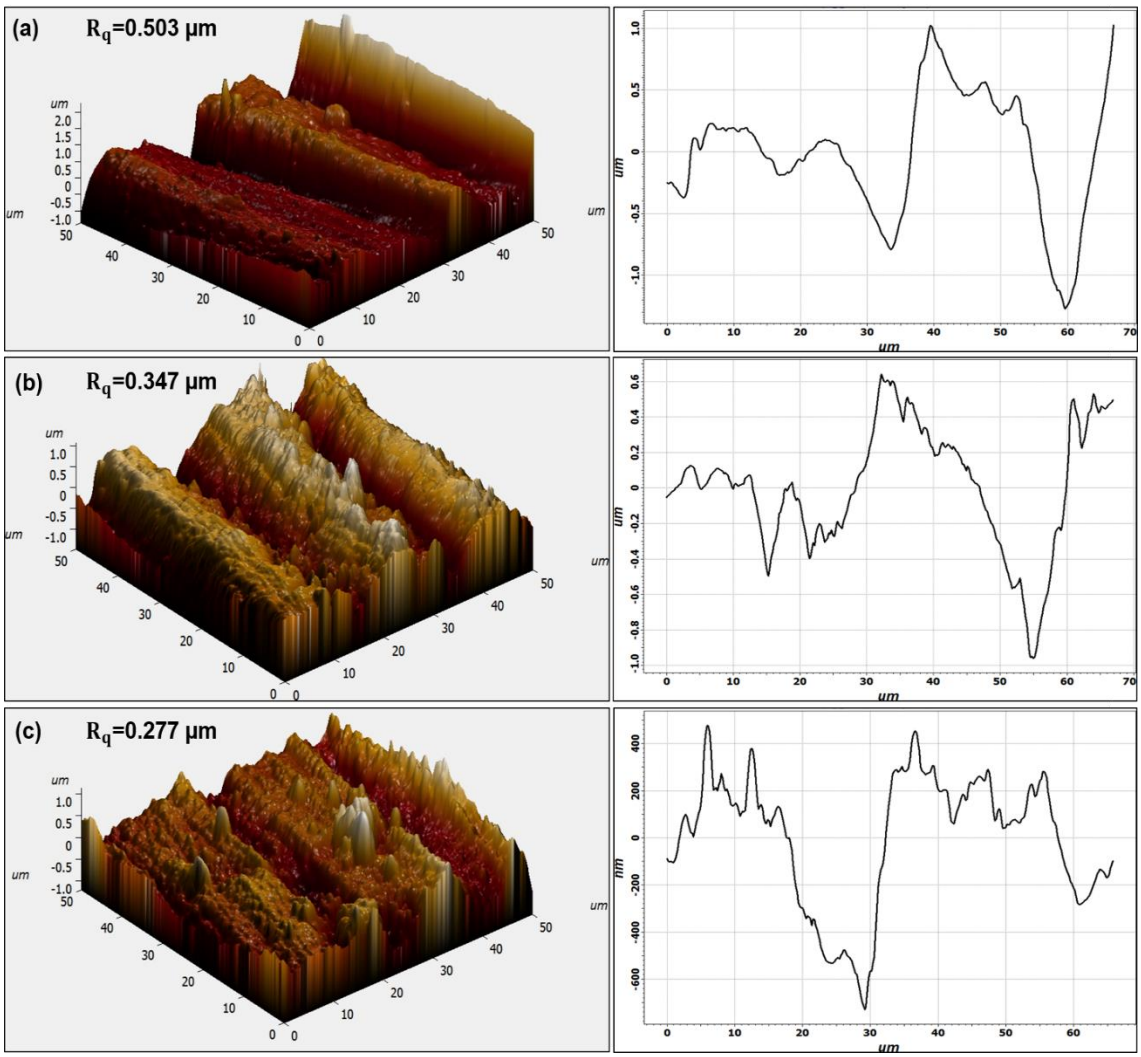

Figure 3.40 AFM morphology of worn surfaces at sliding distance of 2260 m, sliding velocity of 1.3, and applied normal load of 20 N for the different samples (a) as-cast, (b) forged R=1.5 at 400°C, and (c) forged R=2.0 at 400°C

3.3 Summary

The important findings of the above work are summarized below:

1. Severe surface cracks were observed during open die forging of Al-18Si-2.5Cu-0.6Fe alloy at a room as well as at elevated temperature.
2. The impression die forging of the Al-18Si-2.5Cu-0.6Fe alloy at room temperature under lubricated and unlubricated conditions also show severe surface cracks due to strain hardening and stress concentration at the grain boundaries.

3. The impression die forging of Al-18Si-2.5Cu-0.6Fe alloy at elevated temperatures (300, 400 and 500°C) with different aspect ratios (h/d=1.20, 1.00 and 0.80) under lubricated and unlubricated interfacial friction conditions produce crack free and smooth surface forged products. The converging die forging with reduction ratios 1.5 and 2.0 also produces smooth and defect free products at elevated processing temperatures.
4. During impression die forging of Al-18Si-2.5Cu-0.6Fe alloy under lubricated and unlubricated conditions, it is found that the forging load increases with increased deformation. The specimen with the aspect ratio of 0.8 is closest in shape and size to the 0.63 aspect ratio of the impression die setup and due to smaller deformation can be expected to require the least amount of forging load on processing.
5. Due to the high speed of deformation and in turn high axial compressive stresses the hard and brittle silicon-intermetallic particles got fragmented and distributed along with laterally flowing soft aluminum matrix.
6. The impression and converging die compression of the alloy at elevated temperatures lead to refinement in the microstructure of Al-18Si-2.5Cu-0.6Fe alloy. It may be due to precipitation of fine particles and fragmentation of the coarse Si particles and there was the more uniform distribution of such second phase particles in the Al matrix. However, coarsening of the microstructure occurred from processing at 500°C.
7. In impression die, the optical micrographs of the sample forged at 400°C with aspect ratio 1.20 under lubricated condition indicate refinement in microstructure as compared with other aspect ratios 1.00 and 0.80. In general, lubricated conditions show much better surface movement at the interface and in turn improved microstructural features. Whereas the samples forged through the converging die at 400°C with a reduction ratio 2.0 specifically revealed

considerable refinement in microstructure as compared with the reduction ratio 1.50.

8. Higher deformation leads to higher tensile strength and hardness. The bulk deformation at high strain rate with high dislocation density and fine grain distribution strengthens the material and consequently improves these mechanical properties.
9. The optimum properties of the bulk processed alloy like UTS, hardness and wear resistance were observed for the samples forged with the aspect ratio of 1.20 in impression die, and reduction ratio of 2.0 in converging die at 400°C.
10. Adhesion and abrasion were the primary wear mechanisms in both as-cast and forged samples. The wear resistance of the samples processed under compressive load at the elevated temperatures of 300, 400, and 500°C was higher as compared to that of the as-cast alloy. The roughness of the worn out surface of the sample forged at 400°C was found to be minimum and much less than that of the as-cast sample.

The next chapter 4 deals with deformation behavior and tribo-mechanical properties of the complex eutectic Al-11Si-2.5Cu-0.6Fe alloy during forging.